Biochemistry

pubs.acs.org/biochemistry Article

Targeted Degradation of the Oncogenic Phosphatase SHP2

Vidyasiri Vemulapalli, Katherine A. Donovan, Tom C. M. Seegar, Julia M. Rogers, Munhyung Bae, Ryan J. Lumpkin, Ruili Cao, Matthew T. Henke, Soumya S. Ray, Eric S. Fischer, Gregory D. Cuny, and Stephen C. Blacklow*

Cite This: *Biochemistry* 2021, 60, 2593–2609 Read Online

ACCESS | Metrics & More | Article Recommendations | Supporting Information

ABSTRACT: SHP2 is a protein tyrosine phosphatase that plays a critical role in the full activation of the Ras-MAPK pathway upon stimulation of receptor tyrosine kinases, which are frequently amplified or mutationally activated in human cancer. In addition, activating mutations in SHP2 result in developmental disorders and hematologic malignancies. Several allosteric inhibitors have been developed for SHP2 and are currently in clinical trials. Here, we report the development and evaluation of a SHP2 PROTAC created by conjugating RMC-4550 with pomalidomide using a PEG linker. This molecule is highly selective for SHP2, induces degradation of SHP2 in leukemic cells at submicromolar concentrations, inhibits MAPK signaling, and suppresses cancer cell growth. SHP2 PROTACs serve as an alternative strategy for targeting ERK-dependent cancers and are useful tools alongside allosteric inhibitors for dissecting the mechanisms by which SHP2 exerts its oncogenic activity.

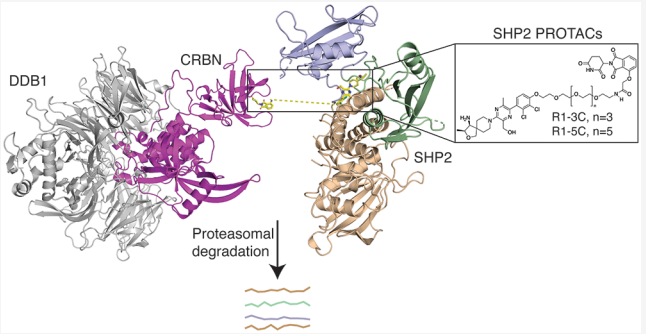

The proto-oncogene PTPN11 encodes a cytoplasmic protein tyrosine phosphatase, SHP2, which is required for normal development. SHP2 acts downstream of multiple receptor tyrosine kinases (RTKs) to exert sustained activation of the RAS-MAPK signaling cascade. The first oncogenic phosphatase to be identified, SHP2 is dysregulated in multiple human diseases, where germline mutations cause the developmental disorders Noonan and LEOPARD syndromes. Somatic mutations of SHP2 are found in ∼35% of cases of juvenile myelomonocytic leukemia (JMML) and are seen recurrently in myelodysplastic syndrome, in ALL, in AML, and even in solid tumors.[1,2] Oncogenic mutations in SHP2 destabilize the "off" or "auto-inhibited" state of the enzyme and increase basal activity by shifting the conformational equilibrium toward a more open state,[3] which leads to uncontrolled MAPK activation. Reduction of SHP2 activity through genetic knockdown or allosteric inhibition suppresses RAS-ERK signaling and inhibits tumor growth, validating SHP2 as a target for cancer therapy.[4] Moreover, because SHP2 lies downstream of the T cell immunoinhibitory receptor PD-1, SHP2 inhibition may also be a viable strategy for cancer immunotherapy in combination with PD-1 blockade or with other immunomodulatory agents.[5−7]

Structurally, SHP2 is composed of two tandem Src homology 2 (SH2) domains, N-SH2 and C-SH2, followed by a catalytic protein tyrosine phosphatase (PTP) domain and an unstructured C-terminal tail. In the basal state, the N-SH2 domain packs against and sterically occludes the active site of the PTP domain by inserting a loop into the cleft that inhibits substrate access. Upon engagement of the N-SH2 and C-SH2 domains of SHP2 with tyrosine-phosphorylated signaling proteins, SHP2 activity is induced, presumably due to an induced conformational opening that alleviates N-SH2 autoinhibition of the PTP domain active site.[8] Cancer mutations typically occur at the interface between the N-SH2 and PTP domains and, in most cases, activate the phosphatase.[8]

Given the importance of SHP2 in cancer therapy, there have been a number of efforts to develop SHP2-selective inhibitors. Early reports described active site-directed competitive inhibitors that had poor selectivity.[9,10] More recently, research groups at Novartis and Revolution Medicines developed allosteric inhibitors that are highly selective for SHP2, called SHP099[4,11] and RMC4550,[12] which were both shown to be effective tool compounds with nanomolar potency and preclinical activity in RTK- and RAS-driven cancers.[4,12] Currently, several SHP2 allosteric inhibitors (TNO155,[13] JAB-3312,[14] RMC-4630,[15] RLY-1971,[16] and ERAS-601) are in phase I/II clinical trials for the treatment of advanced or metastatic solid tumors.

Received: June 2, 2021
Revised: August 9, 2021
Published: August 19, 2021

https://doi.org/10.1021/acs.biochem.1c00377
Biochemistry 2021, 60, 2593−2609

Although allosteric SHP2 inhibitors show clinical promise, recent preclinical studies highlight the potential for the emergence of nonmutational mechanisms of resistance.[17] By acutely depleting the target protein, proteolysis targeting chimeras (PROTACs) have the potential to overcome such resistance mechanisms. By degrading the target protein, they have the additional benefit of eliminating any residual activity of the target protein associated with the inhibitor-bound state.

Here, we report the development and characterization of a PROTAC that is highly selective for degradation of SHP2. Our lead compound consists of a SHP2-binding warhead (RMC-4550) tethered to an IMiD (immunomodulatory drug) derivative using a PEG linker. By increasing the linker length of our first-generation PROTAC, we identified a lead compound that carries out highly selective SHP2 degradation with a low nanomolar DC_{50}, suppresses MAPK signaling, and inhibits cancer cell growth. This SHP2-targeting PROTAC will be a valuable tool for acute depletion of SHP2 in functional studies and will be a starting point for further development of a SHP2-targeting PROTAC therapeutic.

MATERIALS AND METHODS

Chemical Synthesis. The compounds reported herein were synthesized as described below.

*2-(2,6-Dioxopiperidin-3-yl)-4-hydroxyisoindoline-1,3-dione (**S1-1**).* A mixture of 3-aminopiperidine-2,6-dione (19.2 g, 116 mmol, 1.00 equiv), 4-hydroxyisobenzofuran-1,3-dione (21.0 g, 128 mmol, 1.10 equiv), and KOAc (34.3 g, 349 mmol, 3.00 equiv) in AcOH (200 mL) was stirred at 120 °C for 3 h. The reaction mixture was concentrated under reduced pressure to remove the solvent. The residue was diluted with water (250 mL), filtered, washed with water, and concentrated under reduced pressure to give 2-(2,6-dioxopiperidin-3-yl)-4-hydroxyisoindoline-1,3-dione (28.0 g, 101 mmol, 86.7% yield, 98.8% purity) as a gray solid (Scheme 1).

Scheme 1

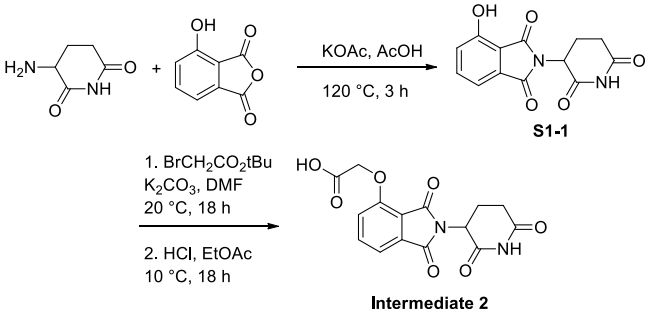

*2-{[2-(2,6-Dioxopiperidin-3-yl)-1,3-dioxoisoindolin-4-yl]-oxy}acetic Acid (intermediate **2**).* To a solution of 2-(2,6-dioxopiperidin-3-yl)-4-hydroxyisoindoline-1,3-dione (28.0 g, 102 mmol, 1.00 equiv) in DMF (200 mL) were added *tert*-butyl 2-bromoacetate (19.9 g, 102 mmol, 15.1 mL, 1.00 equiv), KI (1.69 g, 10.2 mmol, 0.100 equiv), and K_2CO_3 (21.2 g, 153 mmol, 1.50 equiv). The mixture was stirred at 20 °C for 18 h. The reaction mixture was diluted with water (250 mL) and extracted with EtOAc (3 × 150 mL). The combined organic layers were washed with saturated NaCl (200 mL), dried over anhydrous Na_2SO_4, filtered, and concentrated under reduced pressure to give a residue. The crude product was triturated with MTBE (200 mL) at 10 °C for 3 h, and then the product was triturated with *n*-heptane (100 mL) at 105 °C for 3 h to give the product *tert*-butyl 2-{[2-(2,6-dioxopiperidin-3-yl)-1,3-dioxoisoindolin-4-yl]oxy}acetate (36.0 g, 90.1 mmol, 88.7% yield, 97.7% purity) as a white solid.

To a solution of *tert*-butyl 2-{[2-(2,6-dioxopiperidin-3-yl)-1,3-dioxoisoindolin-4-yl]oxy}acetate (5.00 g, 12.9 mmol, 1.00 equiv) in EtOAc (2.00 mL) was added HCl/EtOAc (4 M, 45.0 mL, 14.0 equiv). The mixture was stirred at 10 °C for 18 h. The reaction mixture was concentrated under reduced pressure to remove the EtOAc. The crude product was triturated with MTBE (200 mL) at 10 °C for 1 h, filtered, and concentrated under reduced pressure. To the solid was added deionized water (100 mL). The residual aqueous solution was lyophilized to give intermediate **2** (4.00 g, 11.6 mmol, 90.3% yield, 96.6% purity) as a white solid.

*(4-Amino-2,3-dichlorophenyl)methanol (**S2-1**).* To a solution of methyl 4-amino-2-chlorobenzoate (72.0 g, 387 mmol, 1.00 equiv) in DMF (360 mL) was added NCS (55.0 g, 411 mmol, 1.06 equiv) at 0 °C, and the mixture was stirred at 40 °C for 24 h. The reaction mixture was poured into water (500 mL), and a precipitate was formed, filtered, and collected. The crude product was purified by recrystallization from EtOH (250 mL) at 80 °C to give methyl 4-amino-2,3-dichlorobenzoate (48.0 g, 56.2% yield) as a yellow solid (Scheme 2).

To a solution of 4-amino-2,3-dichlorobenzoate (50.0 g, 227 mmol, 1.00 equiv) in THF (500 mL) was added $LiAlH_4$ (18.0 g, 474 mmol, 2.09 equiv) at 0 °C, and the mixture was stirred at 0 °C for 2 h. To the mixture were slowly added water (23 mL), 15% NaOH (23 mL), and $MgSO_4$ (150 g) at 0 °C, and the mixture was stirred at 10 °C for 15 min, filtered, and concentrated under reduced pressure to give a residue. The mixture was triturated with petroleum ether/EtOAc (6/1, 70 mL) at 15 °C for 12 h to give **S2-1** (36.0 g, 75.9% yield, 92.1% purity) as a light yellow solid.

*Methyl 2-(2,3-Dichloro-4-iodophenyl)acetate (**S2-2**).* To a solution of **S2-1** (34.0 g, 177 mmol, 1.00 equiv) in H_2O (340 mL) and HCl (12 M, 340 mL, 23.0 equiv) was added dropwise a solution of $NaNO_2$ (18.3 g, 265 mmol, 1.50 equiv) in water (34 mL) at 0 °C. The mixture was stirred at 0 °C for 30 min. Then a solution of KI (146 g, 885 mmol, 5.00 equiv) in water (340 mL) was added dropwise at 0 °C, and the resulting mixture was stirred at 0 °C for 30 min. The mixture was extracted with EtOAc (3 × 600 mL). The combined organic phase was washed with brine and dried over anhydrous Na_2SO_4, filtered, and concentrated under vacuum to give a residue. The residue was purified by column chromatography (SiO_2, petroleum ether/EtOAc from 100/1 to 20/1, R_f = 0.56) to give (2,3-dichloro-4-iodophenyl)methanol (25.0 g, 46.6% yield) as a yellow solid.

To a solution of (2,3-dichloro-4-iodophenyl)methanol (26.0 g, 85.8 mmol, 1.00 equiv) in DCM (500 mL) and TEA (26.0 g, 257 mmol, 35.8 mL, 3.00 equiv) was added MsCl (13.2 g, 115 mmol, 8.95 mL, 1.35 equiv) at 0 °C. The mixture was stirred at 0 °C for 1 h. The mixture was washed with brine (3 × 300 mL) and dried over anhydrous Na_2SO_4, filtered, and concentrated under vacuum to give the corresponding mesylate (31.0 g, 94.7% yield) as a brown solid. To this material (31.0 g, 81.3 mmol, 1.00 equiv) in EtOH (620 mL) was added a solution of NaCN (6.04 g, 123 mmol, 1.51 equiv) in water (155 mL). The mixture was stirred at 80 °C for 8 h. The mixture was concentrated under vacuum to remove EtOH, diluted with water (150 mL), and extracted with EtOAc (3 × 100 mL). The combined organic phase was washed with brine (200 mL) and dried over anhydrous Na_2SO_4, filtered, and concentrated under vacuum

https://doi.org/10.1021/acs.biochem.1c00377
Biochemistry 2021, 60, 2593−2609

Scheme 2

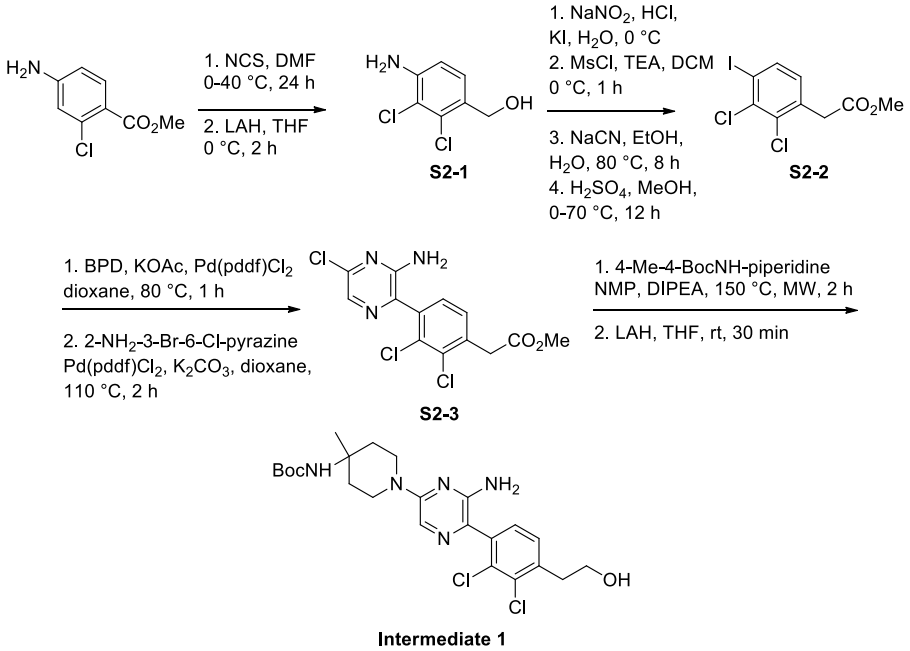

to give 2-(2,3-dichloro-4-iodophenyl)acetonitrile (18.0 g, 70.9% yield) as a light yellow solid.

To a solution of 2-(2,3-dichloro-4-iodophenyl)acetonitrile (17.0 g, 54.5 mmol, 1.00 equiv) in MeOH (150 mL) was added H_2SO_4 (88.3 g, 900 mmol, 48.0 mL, 16.5 equiv) at 0 °C. The mixture was stirred at 70 °C for 12 h. The reaction mixture was concentrated under reduced pressure to remove MeOH. The residue was diluted with water (150 mL) and extracted with EtOAc (2 × 100 mL). The combined organic layers were washed with brine (200 mL), dried over anhydrous Na_2SO_4, filtered, and concentrated under reduced pressure to give **S2-2** (15.0 g, 79.7% yield) as a light yellow solid.

*Methyl 2-[4-(3-Amino-5-chloropyrazin-2-yl)-2,3-dichlorophenyl]acetate (**S2-3**).* A mixture of **S2-2** (6.00 g, 17.3 mmol, 1.00 equiv), BPD (4.64 g, 18.2 mmol, 1.05 equiv), AcOK (8.54 g, 86.9 mmol, 5.00 equiv), and Pd(dppf)Cl_2 (600 mg, 920 μmol, 5.29 × 10^{-2} equiv) in 1,4-dioxane (60 mL) was stirred at 80 °C for 1 h under N_2. The mixture was filtered, and the filtrate was concentrated under vacuum to give a residue. The residue was purified by column chromatography (SiO_2, petroleum ether/EtOAc from 30/1 to 10/1, R_f = 0.54, I_2) to give methyl 2-[2,3-dichloro-4-(4,4,5,5-tetramethyl-1,3,2-dioxaborolan-2-yl)phenyl]acetate (5.50 g, crude) as a light yellow oil.

A mixture of 3-bromo-6-chloropyrazin-2-amine (1.00 g, 4.80 mmol, 1.00 equiv), methyl 2-[2,3-dichloro-4-(4,4,5,5-tetramethyl-1,3,2-dioxaborolan-2-yl)phenyl]acetate (4.97 g, 14.3 mmol, 3.00 equiv), Pd(dppf)Cl_2 (175 mg, 239 μmol, 0.05 equiv), and K_2CO_3 (663 mg, 4.80 mmol, 1.00 equiv) in 1,4-dioxane (40 mL) was stirred at 110 °C for 2 h. The mixture was filtered through a pad of Celite, and the filtrate was concentrated under vacuum to give a residue. The residue was purified by column chromatography (SiO_2, petroleum ether/EtOAc from 30/1 to 1/1, R_f = 0.23) to give **S2-3** (900 mg, 51.3% yield, 94.8% purity) as a yellow solid.

*tert-Butyl (1-{6-Amino-5-[2,3-dichloro-4-(2-hydroxyethyl)-phenyl]pyrazin-2-yl}-4-methylpiperidin-4-yl)carbamate (intermediate **1**).* **S2-3** (900 mg, 2.46 mmol, 1.00 equiv), *tert*-butyl (4-methylpiperidin-4-yl)carbamate (800 mg, 3.73 mmol, 1.52 equiv), and DIPEA (1.59 g, 12.3 mmol, 2.14 mL, 5.00 equiv) were taken up into a microwave tube in NMP (10 mL). The sealed tube was heated at 150 °C for 2 h under microwave. The mixture was diluted with water (30 mL) and extracted with EtOAc (3 × 30 mL). The combined organic phase was washed with brine (50 mL) and dried over anhydrous Na_2SO_4, filtered, and concentrated under vacuum to give a residue. The residue was purified by column chromatography (SiO_2, petroleum ether/EtOAc from 10/1 to 1/1, R_f = 0.33) to give methyl 2-[4-(3-amino-5-{4-[(*tert*-butoxycarbonyl)amino]-4-methylpiperidin-1-yl}pyrazin-2-yl)-2,3-dichlorophenyl]acetate (600 mg, 40.5% yield, 87.3% purity) as a yellow oil.

To a solution of methyl 2-[4-(3-amino-5-{4-[(*tert*-butoxycarbonyl)amino]-4-methylpiperidin-1-yl}pyrazin-2-yl)-2,3-dichlorophenyl]acetate (600 mg, 998 μmol, 1.00 equiv) in THF (1.5 mL) was added $LiAlH_4$ (78.5 mg, 2.07 mmol, 2.07 equiv). The mixture was stirred at 20 °C for 0.5 h. Next, 0.08 mL of water and 0.08 mL of 10% aqueous NaOH were added to the mixture at 0 °C, followed by the addition 0.24 mL of water and 3.00 g of $MgSO_4$. The mixture was stirred at 15 °C for 15 min and filtered, and the filtrate was concentrated under vacuum to give a residue. The residue was purified by column chromatography (SiO_2, petroleum ether/EtOAc from 10/1 to 1/1, R_f = 0.23) to give intermediate **1** (400 mg, 74.0% yield, 91.8% purity) as a yellow oil.

*3,4-Dichloro-5-[(4-methoxybenzyl)oxy]benzaldehyde (**S3-1**).* To a solution of 4-methoxybenzyl alcohol (PMBOH, 30.5 g, 221 mmol, 27.5 mL, 1.20 equiv) in THF (450 mL) was added NaH (10.3 g, 258 mmol, 60% purity, 1.40 equiv) at 25 °C. The mixture was stirred at 25 °C for 0.5 h. Then 5-bromo-1,2-dichloro-3-fluorobenzene (45.0 g, 184 mmol, 1.00 equiv) was added, and the resulting mixture was stirred at 25 °C for 16 h. The reaction was quenched with 600 mL of saturated aqueous NH_4Cl, and the mixture extracted with EtOAc (3 × 500 mL). The combined organic phase was washed with 800 mL of brine and dried over anhydrous Na_2SO_4, filtered, and concentrated under vacuum to give a residue. The residue was purified by flash silica gel chromatography (ISCO; 80.0 g SepaFlash Silica Flash

https://doi.org/10.1021/acs.biochem.1c00377
Biochemistry 2021, 60, 2593−2609

Scheme 3

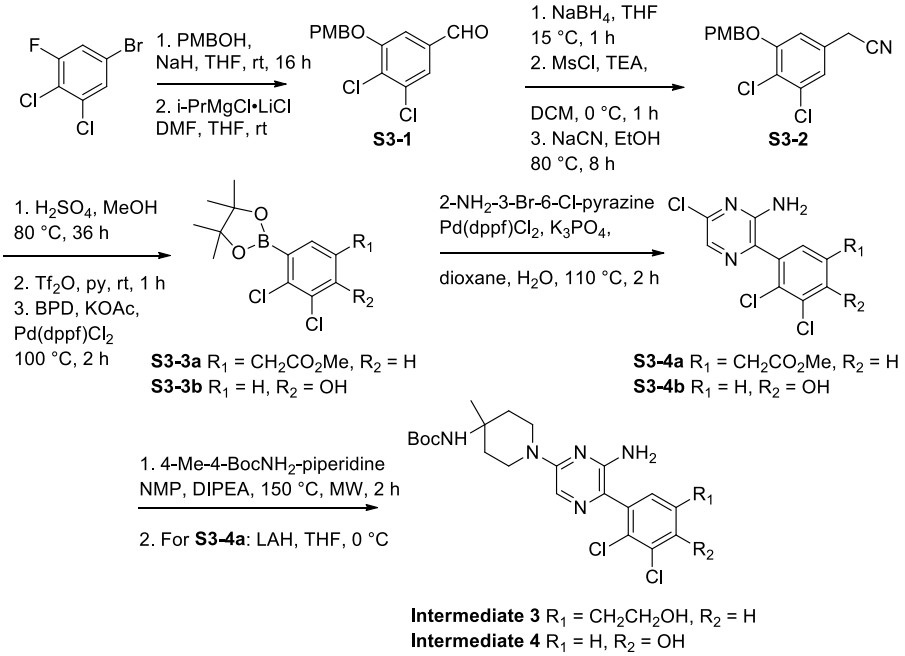

Column; eluent, 0% to 4% EtOAc/petroleum ether gradient) to give 5-bromo-1,2-dichloro-3-[(4-methoxybenzyl)oxy]benzene (60.0 g, 89.8% yield) as a white solid (Scheme 3).

To a solution of 5-bromo-1,2-dichloro-3-[(4-methoxybenzyl)oxy]benzene (59.0 g, 162 mmol, 1.00 equiv) in THF (600 mL) was added i-PrMgCl·LiCl (1.3 M, 250 mL, 2.00 equiv) at 0 °C. The mixture was stirred at 25 °C for 2 h. Then DMF (35.7 g, 488 mmol, 37.6 mL, 3.00 equiv) was added dropwise, and the resulting mixture was stirred at 25 °C for 1 h. The reaction was quenched with 500 mL of saturated aqueous NH_4Cl and extracted with EtOAc (3 × 400 mL). The combined organic phase was washed with 500 mL of brine and dried over anhydrous Na_2SO_4, filtered, and concentrated under vacuum to give a residue. The residue was triturated with 150 mL of petroleum ether at 25 °C for 8 h and then filtered to afford **S3-1** (48.0 g, 94.6% yield) as a white solid.

*2-{3,4-Dichloro-5-[(4-methoxybenzyl)oxy]phenyl}-acetonitrile (**S3-2**).* To a solution of **S3-1** (48.0 g, 154 mmol, 1.00 equiv) in THF (500 mL) was added $NaBH_4$ (11.6 g, 307 mmol, 2.00 equiv) at 0 °C, and the mixture was stirred at 15 °C for 1 h. The reaction was quenched with 400 mL of water, and the mixture extracted with EtOAc (3 × 300 mL). The combined organic phase was washed with 500 mL of brine and dried over anhydrous Na_2SO_4, filtered, and concentrated under vacuum to give {3,4-dichloro-5-[(4-methoxybenzyl)oxy]phenyl}methanol (46.0 g, 95.2% yield) as a light yellow solid.

To a solution of {3,4-dichloro-5-[(4-methoxybenzyl)oxy]-phenyl}methanol (46.0 g, 146 mmol, 1.00 equiv) in Et_3N (44.5 g, 440 mmol, 61.3 mL, 3.00 equiv) and DCM (500 mL) was added MsCl (23.7 g, 207 mmol, 16.0 mL, 1.41 equiv) at 0 °C. Then the mixture was stirred at 0 °C for 1 h. The reaction mixture was washed with brine (3 × 400 mL) and dried over anhydrous Na_2SO_4, filtered, and concentrated under vacuum to give the corresponding mesylate (37.0 g, 64.3% yield) as a yellow oil. To a solution of the mesylate (37.0 g, 94.5 mmol, 1.00 equiv) in EtOH (740 mL) was added a solution of NaCN (8.59 g, 175 mmol, 1.85 equiv) in water (185 mL) at 25 °C. The mixture was stirred at 80 °C for 8 h. The reaction mixture was concentrated under vacuum to remove EtOH and extracted with EtOAc (3 × 200 mL). The combined organic phase was washed with 300 mL of brine and dried over anhydrous Na_2SO_4, filtered, and concentrated under vacuum to give a residue. The residue was purified by column chromatography (SiO_2, petroleum ether/EtOAc from 20/1 to 3/1, R_f = 0.38) to give **S3-2** (16.5 g, 54.1% yield) as a white solid.

*Methyl 2-[3,4-Dichloro-5-(4,4,5,5-tetramethyl-1,3,2-dioxaborolan-2-yl)phenyl]acetate (**S3-3a**).* To a solution of 2-{3,4-dichloro-5-[(4-methoxybenzyl)oxy]phenyl}acetonitrile (16.0 g, 49.6 mmol, 1.00 equiv) in MeOH (192 mL) was added H_2SO_4 (117 g, 1.20 mol, 64.0 mL, 24.1 equiv) at 0 °C. The mixture was stirred at 80 °C for 36 h. The mixture was poured into 600 mL of saturated $NaHCO_3$ and extracted with EtOAc (3 × 300 mL). The combined organic phase was washed with 500 mL of brine and dried over anhydrous Na_2SO_4, filtered, and concentrated under vacuum to give a residue. The residue was purified by flash silica gel chromatography (ISCO; 18.0 g SepaFlash Silica Flash Column; eluent, 0% to 30% EtOAc/petroleum ether gradient; R_f = 0.23) to give methyl 2-(3,4-dichloro-5-hydroxyphenyl)acetate (9.30 g, 79.6% yield) as a white solid.

To a solution of methyl 2-(3,4-dichloro-5-hydroxyphenyl)-acetate (8.20 g, 34.8 mmol, 1.00 equiv) in pyridine (50 mL) was added Tf_2O (10.8 g, 38.3 mmol, 6.33 mL, 1.10 equiv) at 0 °C. The mixture was stirred at 20 °C for 1 h. The reaction mixture was diluted with 150 mL of EtOAc and washed with 1 N HCl (2 × 100 mL). The organic phase was washed with brine (2 × 100 mL) and dried over anhydrous Na_2SO_4, filtered, and concentrated under vacuum to give the triflate (12.5 g, crude) as a yellow oil. To a solution of the triflate (12.5 g, 34.0 mmol, 1.00 equiv) in 1,4-dioxane (130 mL) were added bis-(pinacolato)diboron (BPD, 8.65 g, 34.0 mmol, 1.00 equiv), $Pd(dppf)Cl_2$ (2.50 g, 3.42 mmol, 0.10 equiv), and KOAc (10.0 g, 102 mmol, 3.00 equiv) under N_2. The mixture was stirred at 100 °C for 2 h. The mixture was filtered through a pad of Celite, and the filtrate was concentrated under vacuum to give a residue. The residue was purified by column chromatography (SiO_2,

https://doi.org/10.1021/acs.biochem.1c00377
Biochemistry 2021, 60, 2593−2609

Scheme 4

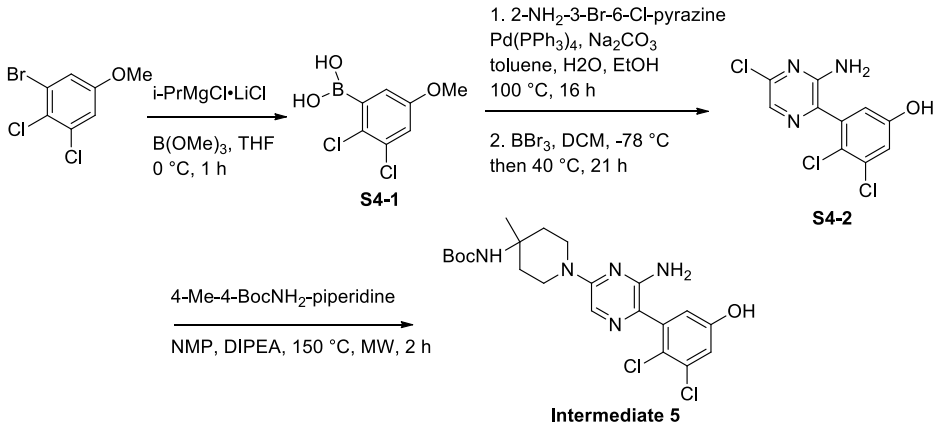

petroleum ether/EtOAc from 20/1 to 4/1, R_f = 0.54) to give **S3-3a** (15.0 g, crude) as a yellow oil.

*Methyl 2-[3-(3-Amino-5-chloropyrazin-2-yl)-4,5-dichlorophenyl]acetate (**S3-4a**).* To a solution of **S3-3a** (14.9 g, 43.1 mmol, 1.50 equiv) in 1,4-dioxane (160 mL) were added 3-bromo-6-chloropyrazin-2-amine (6.00 g, 28.7 mmol, 1.00 equiv), Pd(dppf)Cl_2 (2.11 g, 2.88 mmol, 0.10 equiv), and K_3PO_4 (13.0 g, 61.2 mmol, 2.13 equiv) under N_2. The mixture was stirred at 110 °C for 2 h. The reaction mixture was filtered through a pad of Celite, and the filtrate was concentrated under vacuum to give a residue. The residue was purified by column chromatography (SiO_2, petroleum ether/EtOAc from 15/1 to 1/1; TLC, 2/1 petroleum ether/EtOAc, R_f = 0.45) to give **S3-4a** (9.00 g, 90.2% yield) as a yellow solid.

*tert-Butyl (1-{6-Amino-5-[2,3-dichloro-5-(2-hydroxyethyl)-phenyl]pyrazin-2-yl}-4-methylpiperidin-4-yl)carbamate (intermediate **3**).* To a solution of **S3-4** (1.20 g, 3.46 mmol, 1.00 equiv) in NMP (10 mL) were added *tert*-butyl (4-methylpiperidin-4-yl)carbamate (840 mg, 3.92 mmol, 1.13 equiv) and DIPEA (2.24 g, 17.3 mmol, 3.02 mL, 5.00 equiv). The suspension was degassed and purged with N_2 three times and stirred at 150 °C for 2 h under microwave. The reaction mixture was diluted with 100 mL of water and extracted with EtOAc (3 × 60 mL). The combined organic phase was washed with brine (3 × 100 mL) and dried over anhydrous Na_2SO_4, filtered, and concentrated under vacuum to give a residue. The residue was purified by flash silica gel chromatography (ISCO; 12.0 g SepaFlash Silica Flash Column; eluent, 0% to 50% EtOAc/petroleum ether gradient; R_f = 0.38) to give methyl 2-[3-(3-amino-5-{4-[(*tert*-butoxycarbonyl)amino]-4-methylpiperidin-1-yl}pyrazin-2-yl)-4,5-dichlorophenyl]acetate (2.60 g, crude) as a yellow solid.

To a solution of methyl 2-[3-(3-amino-5-{4-[(*tert*-butoxycarbonyl)amino]-4-methylpiperidin-1-yl}pyrazin-2-yl)-4,5-dichlorophenyl]acetate (2.50 g, 4.77 mmol, 1.00 equiv) in THF (30 mL) was added $LiAlH_4$ (181 mg, 4.77 mmol, 1.00 equiv) at 0 °C, and the mixture was stirred at 0 °C for 0.5 h. The reaction was quenched with 0.15 mL of water, 0.15 mL of 15% NaOH, and 0.3 mL of water at 0 °C. Next, 2.00 g of $MgSO_4$ was added. The mixture was stirred at 25 °C for 30 min and then filtered through a pad of Celite, and the filtrate was concentrated under vacuum to give a residue. The residue was purified by reversed-phase HPLC (0.1% formic acid condition) to give intermediate **3** (650 mg, 27.4% yield) as a yellow foam.

*2,3-Dichloro-4-(4,4,5,5-tetramethyl-1,3,2-dioxaborolan-2-yl)phenol (**S3-3b**).* To a solution of 2,3-dichlorophenol (40.0 g, 245 mmol, 1.00 equiv) in DCM (200 mL) was added Br_2 (43.1 g, 270 mmol, 13.9 mL, 1.10 equiv) over 30 min at 0 °C. The mixture was warmed to 15 °C for 16 h. The mixture was washed with 10% aqueous Na_2SO_3 (240 mL) and then washed with brine (120 mL). The combined water phase was washed with DCM (150 mL). The combined organic phase was dried over anhydrous Na_2SO_4, filtered, and concentrated under reduced pressure to give a residue. The residue was purified by column chromatography (SiO_2, petroleum ether/EtOAc from 100/1 to 0/1) to give 4-bromo-2,3-dichlorophenol (25.7 g, 106 mmol, 43.3% yield, 100% purity) as an off-white solid.

To a solution of 4-bromo-2,3-dichlorophenol (4.00 g, 16.5 mmol, 1.00 equiv), BPD (5.46 g, 21.5 mmol, 2.53 mL, 1.30 equiv), and AcOK (4.87 g, 49.6 mmol, 3.00 equiv) in 1,4-dioxane (40.0 mL) was added Pd(dppf)Cl_2·DCM (1.08 g, 1.32 mmol, 0.08 equiv) under N_2. The mixture was stirred at 90 °C for 15 h. The reaction mixture was filtered; the residue was washed with EtOAc (4 × 100 mL), and the filtrate was concentrated. The residue was purified by column chromatography (SiO_2, petroleum ether/EtOAc from 100/1 to 10/1; TLC, 5/1 petroleum ether/EtOAc, R_f = 0.49) to give **S3-3b** (2.50 g, 8.10 mmol, 49.0% yield, 93.6% purity) as a white solid.

*4-(3-Amino-5-chloropyrazin-2-yl)-2,3-dichlorophenol (**S3-4b**).* The following reactions were performed twice. To a solution of 3-bromo-6-chloropyrazin-2-amine (731 mg, 3.51 mmol, 1.00 equiv) and **S3-3b** (1.30 g, 4.21 mmol, 1.20 equiv) in water (2.00 mL) and 1,4-dioxane (8.00 mL) were added K_3PO_4 (2.61 g, 12.3 mmol, 3.50 equiv) and Pd(dppf)Cl_2 (128 mg, 175 μmol, 0.05 equiv). The reaction mixture was stirred at 110 °C for 1.5 h. The reaction mixture was filtered and concentrated under reduced pressure to give a residue. The residue was diluted with water (10.0 mL) and extracted with EtAcO (2 × 10.0 mL). The combined organic layers were washed with brine (20.0 mL), dried over anhydrous Na_2SO_4, filtered, and concentrated under reduced pressure to give a residue. The two batches were combined for purification by prep-HPLC (neutral condition) to give **S3-4b** (1.03 g, 3.51 mmol, 78.5% yield, 99.0% purity) as a yellow solid.

*tert-Butyl {1-[6-Amino-5-(2,3-dichloro-4-hydroxyphenyl)-pyrazin-2-yl]-4-methylpiperidin-4-yl}carbamate (intermediate **4**).* **S3-4b** (1.03 g, 3.51 mmol, 1.00 equiv), *tert*-butyl (4-methylpiperidin-4-yl)carbamate (1.13 g, 5.26 mmol, 1.50 equiv), and DIPEA (2.27 g, 17.6 mmol, 3.06 mL, 5.00 equiv) were taken up into a microwave tube in NMP (10.0 mL). The sealed tube was heated at 150 °C for 2 h under microwave. The mixture was partitioned between water (20.0 mL) and EtOAc

https://doi.org/10.1021/acs.biochem.1c00377
Biochemistry 2021, 60, 2593−2609

(20.0 mL). The water phase was separated and washed with EtOAc (4 × 20.0 mL). The combined organic phase was washed with brine (10.0 mL), dried over anhydrous Na_2SO_4, filtered, and concentrated under reduced pressure to give a residue. The residue was purified by prep-HPLC (neutral condition) to give intermediate **4** (700 mg, 1.39 mmol, 39.7% yield, 93.3% purity) as a brown solid.

*(2,3-Dichloro-5-methoxyphenyl)boronic acid (**S4-1**).* To a solution of 1-bromo-2,3-dichloro-5-methoxybenzene (5.00 g, 19.2 mmol, 1.00 equiv) in THF (100 mL) was added dropwise i-PrMgCl·LiCl (1.30 M, 23.9 mL, 1.62 equiv) at 0 °C under N_2. The mixture was stirred at 0 °C for 1 h. Then trimethyl borate (9.95 g, 95.8 mmol, 10.8 mL, 5.00 equiv) was added at 0 °C, and the mixture stirred for 1 h. Next, HCl (1.00 M, 51.5 mL, 2.69 equiv) was added, and the mixture stirred at 0 °C for 1 h. The organic phase was separated, filtered, and concentrated under reduced pressure to give a residue **S4-1** (4.90 g, 17.9 mmol, 93.6% yield, 80.8% purity) as a white solid (Scheme 4).

*3-(3-Amino-5-chloropyrazin-2-yl)-4,5-dichlorophenol (**S4-2**).* To a mixture of **S4-1** (2.00 g, 7.32 mmol, 1.20 equiv), 3-bromo-6-chloropyrazin-2-amine (1.27 g, 6.10 mmol, 1.00 equiv), $Pd(PPh_3)_4$ (564 mg, 488 μmol, 0.080 equiv), and Na_2CO_3 (1.29 g, 12.20 mmol, 2.00 equiv) in toluene (10.0 mL) were added water (2.00 mL) and EtOH (4.00 mL). Then the mixture was degassed and purged with N_2 three times. The mixture was stirred at 100 °C for 16 h under a N_2 atmosphere. The reaction mixture was partitioned between ethyl acetate (100 mL) and water (80.0 mL). The water phase was separated and washed with ethyl acetate (3 × 100 mL). The combined organic phase was washed with brine (2 × 60.0 mL), dried over anhydrous Na_2SO_4, filtered, and concentrated under reduced pressure to give a residue. The residue was purified by column chromatography (SiO_2, petroleum ether/EtOAc from 20/1 to 3/1; TLC, 3/1 petroleum ether/EtOAc, R_f = 0.62) to give 6-chloro-3-(2,3-dichloro-5-methoxyphenyl)pyrazin-2-amine (1.70 g, 5.24 mmol, 86.0% yield, 93.9% purity) as a yellow solid.

To a solution of 6-chloro-3-(2,3-dichloro-5-methoxyphenyl)-pyrazin-2-amine (1.70 g, 5.24 mmol, 1.00 equiv) in DCM (85.0 mL) was added dropwise BBr_3 (1 M, 10.5 mL, 2.00 equiv) at −78 °C over 1 h. After the addition, the resulting mixture was stirred at 40 °C for 21 h. The mixture was poured into ice/water (150 mL) and washed with DCM (3 × 100 mL). The combined organic phase was washed with brine (100 mL), dried over anhydrous Na_2SO_4, filtered, and concentrated under reduced pressure to give a residue. The residue was purified by prep-HPLC (TFA condition) to give **S4-2** (370 mg, 1.19 mmol, 22.7% yield, 93.5% purity) as a yellow solid.

*tert-Butyl {1-[6-Amino-5-(2,3-dichloro-5-hydroxyphenyl)-pyrazin-2-yl]-4-methylpiperidin-4-yl}carbamate (intermediate **5**).* **S4-2** (520 mg, 1.79 mmol, 1.00 equiv), *tert*-butyl (4-methylpiperidin-4-yl)carbamate (575 mg, 2.68 mmol, 1.50 equiv), and DIPEA (1.16 g, 8.95 mmol, 1.56 mL, 5.00 equiv) were taken up into a microwave tube in NMP (5.00 mL). The sealed tube was heated at 150 °C for 2 h under microwave. The combined mixture was partitioned between water (20.0 mL) and EtOAc (20.0 mL). The water phase was separated and washed with EtOAc (4 × 20.0 mL). The combined organic phase was washed with brine (3 × 10.0 mL), dried over anhydrous Na_2SO_4, filtered, and concentrated under reduced pressure to give a residue. The residue was purified by column chromatography (SiO_2, petroleum ether/EtOAc from 10/1 to 1/1; TLC, 1/1 petroleum ether/EtOAc, R_f = 0.40) to give intermediate **5** (450 mg, 888 μmol, 49.6% yield, 92.4% purity) as a yellow oil.

*Synthesis of **S9-1c**.* To a solution of intermediate **1** (100 mg, 184 μmol, 1.00 equiv) in THF (1.5 mL) was added NaH (15.0 mg, 375 μmol, 60% purity, 2.03 equiv) at 0 °C, followed by the addition of 14-azido-3,6,9,12-tetraoxatetradecyl 4-methylbenzenesulfonate (100 mg, 239 μmol, 1.30 equiv). The mixture was stirred at 60 °C for 3 h. The reaction was quenched with water (2 mL), and the mixture extracted with EtOAc (3 × 2 mL). The combined organic phase was concentrated under vacuum to give a residue. The residue was purified by prep-TLC (10/1 dichloromethane/methanol; TLC, 10/1 dichloromethane/methanol, R_f = 0.55) to give *tert*-butyl (1-{6-amino-5-[4-(17-azido-3,6,9,12,15-pentaoxaheptadecyl)-2,3-dichlorophenyl]-pyrazin-2-yl}-4-methylpiperidin-4-yl)carbamate (50.0 mg, 34.0% yield, 93.4% purity) as a yellow oil (Scheme 5).

Scheme 5

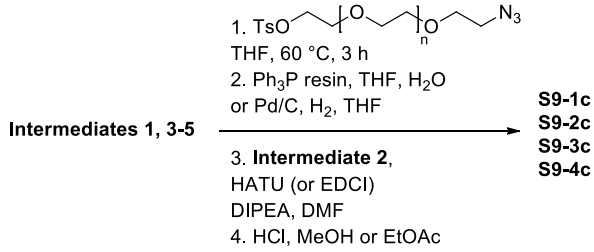

To a solution of *tert*-butyl (1-{6-amino-5-[4-(17-azido-3,6,9,12,15-pentaoxaheptadecyl)-2,3-dichlorophenyl]pyrazin-2-yl}-4-methylpiperidin-4-yl)carbamate (40.0 mg, 50.3 μmol, 1.00 equiv) in THF (1 mL) and water (0.3 mL) was added PPh_3 (13.2 mg, 50.3 μmol, 1.00 equiv). The mixture was stirred at 60 °C for 3 h. The mixture was diluted with 5 mL of EtOAc and washed with 5 mL of brine. The organic phase was concentrated under vacuum to give a residue. The residue was purified by prep-TLC (10/1 dichloromethane/methanol; TLC, 10/1 dichloromethane/methanol, R_f = 0.11) to give *tert*-butyl (1-{6-amino-5-[4-(17-amino-3,6,9,12,15-pentaoxaheptadecyl)-2,3-dichlorophenyl]pyrazin-2-yl}-4-methylpiperidin-4-yl)-carbamate (25.0 mg, 69.3% yield) as a yellow oil.

A mixture of *tert*-butyl (1-{6-amino-5-[4-(17-amino-3,6,9,12,15-pentaoxaheptadecyl)-2,3-dichlorophenyl]pyrazin-2-yl}-4-methylpiperidin-4-yl)carbamate (25.0 mg, 34.9 μmol, 1.00 equiv), intermediate **2** (19.3 mg, 52.4 μmol, 1.50 equiv), HATU (19.9 mg, 52.4 μmol, 1.50 equiv), and DIPEA (13.5 mg, 104 μmol, 18.2 μL, 3.00 equiv) in DMF (1 mL) was stirred at 25 °C for 0.5 h. The mixture was acidified to pH ∼6 with 1 M HCl and purified by prep-HPLC [column, Phenomenex Synergi C18 150 μm × 25 μm × 10 μm; mobile phase, water (0.05% HCl)/acetonitrile; B%, 48% to 68%, 10 min] and lyophilized to give *tert*-butyl (1-{6-amino-5-[2,3-dichloro-4-(1-{[2-(2,6-dioxopiperidin-3-yl)-1,3-dioxoisoindolin-4-yl]oxy}-2-oxo-6,9,12,15,18-pentaoxa-3-azaicosan-20-yl)phenyl}pyrazin-2-yl}-4-methylpiperidin-4-yl)carbamate (15.0 mg, 41.6% yield) as a yellow solid.

A mixture of *tert*-butyl (1-{6-amino-5-[2,3-dichloro-4-(1-{[2-(2,6-dioxopiperidin-3-yl)-1,3-dioxoisoindolin-4-yl]oxy}-2-oxo-6,9,12,15,18-pentaoxa-3-azaicosan-20-yl)phenyl]pyrazin-2-yl}-4-methylpiperidin-4-yl)carbamate (15.0 mg, 14.5 μmol, 1.00 equiv) in HCl-1,4-dioxane (4 M, 0.2 mL, 54.9 equiv) and EtOAc (0.2 mL) was stirred at 20 °C for 0.5 h. The mixture was concentrated under vacuum to give a residue. The residue was

https://doi.org/10.1021/acs.biochem.1c00377
Biochemistry 2021, 60, 2593−2609

purified by prep-HPLC [column, Phenomenex Synergi C18 150 μm × 25 μm × 10 μm; mobile phase, water (0.05% HCl)/acetonitrile; B%, 22% to 42%, 9.5 min] and lyophilized to give **S9-1c** (2.89 mg, 20.3% yield, 95.3% purity) as a yellow solid.

Synthesis of ***S9-2c.*** The following reactions were performed three times. To a solution of intermediate **3** (50.0 mg, 100 μmol, 1.00 equiv) in THF (1 mL) was added NaH (8.06 mg, 201 μmol, 60% purity, 2.00 equiv) at 0 °C, and the mixture was stirred at 40 °C for 1 h. 14-Azido-3,6,9,12-tetraoxatetradecyl 4-methylbenzenesulfonate (45.1 mg, 120 μmol, 1.20 equiv) was added to the reaction mixture at 0 °C. The resulting mixture was stirred at 55 °C for 1 h. The reaction was quenched with 10 mL of saturated NH_4Cl. The three reaction batches were combined, and the resulting mixture was extracted with EtOAc (3 × 10 mL). The combined organic phase was washed with 30 mL of brine and dried over Na_2SO_4, filtered, and concentrated under vacuum to give a residue. The residue was purified by reversed-phase HPLC (0.1% FA condition) to give *tert*-butyl (1-{6-amino-5-[5-(17-azido-3,6,9,12,15-pentaoxaheptadecyl)-2,3-dichlorophenyl]pyrazin-2-yl}-4-methylpiperidin-4-yl)carbamate (60.0 mg, 75.0% purity) as a yellow oil.

A mixture of *tert*-butyl (1-{6-amino-5-[5-(17-azido-3,6,9,12,15-pentaoxaheptadecyl)-2,3-dichlorophenyl]pyrazin-2-yl}-4-methylpiperidin-4-yl)carbamate (58.0 mg, 78.2 μmol, 1.00 equiv) and PPh_3 resin (61.2 mg, 234 μmol, 3.00 equiv) in THF (1 mL) and water (0.3 mL) was stirred at 50 °C for 4 h. The reaction mixture was filtered, and the filtrate was concentrated under vacuum to give *tert*-butyl (1-{6-amino-5-[5-(17-amino-3,6,9,12,15-pentaoxaheptadecyl)-2,3-dichlorophenyl]pyrazin-2-yl}-4-methylpiperidin-4-yl)carbamate (60.0 mg, crude) as a yellow oil.

A mixture of *tert*-butyl (1-{6-amino-5-[5-(17-amino-3,6,9,12,15-pentaoxaheptadecyl)-2,3-dichlorophenyl]pyrazin-2-yl}-4-methylpiperidin-4-yl)carbamate (60.0 mg, 83.8 μmol, 1.00 equiv), intermediate **2** (42.0 mg, 126 μmol, 1.51 equiv), EDCI (28.0 mg, 146 μmol, 1.74 equiv), HOBt (21.0 mg, 155 μmol, 1.85 equiv), and DIPEA (43.0 mg, 332 μmol, 3.97 equiv) in DMF (1 mL) was stirred at 25 °C for 1 h. The reaction mixture was neutralized with 1 M HCl (in DMF) and purified by prep-HPLC [column, Phenomenex Synergi C18 150 μm × 25 μm × 10 μm; mobile phase, water (0.05% HCl)/acetonitrile; B %, 43% to 63%, 8 min] to give *tert*-butyl (1-{6-amino-5-[2,3-dichloro-5-(1-{[2-(2,6-dioxopiperidin-3-yl)-1,3-dioxoisoindolin-4-yl]oxy}-2-oxo-6,9,12,15,18-pentaoxa-3-azaicosan-20-yl)-phenyl]pyrazin-2-yl}-4-methylpiperidin-4-yl)carbamate (45.0 mg, 52.1% yield) as a yellow solid.

A mixture of *tert*-butyl (1-{6-amino-5-[2,3-dichloro-5-(1-{[2-(2,6-dioxopiperidin-3-yl)-1,3-dioxoisoindolin-4-yl]oxy}-2-oxo-6,9,12,15,18-pentaoxa-3-azaicosan-20-yl)phenyl]pyrazin-2-yl}-4-methylpiperidin-4-yl)carbamate (45.0 mg, 43.6 μmol, 1.00 equiv) in MeOH (0.5 mL) and HCl-1,4-dioxane (4 M, 0.5 mL, 45.7 equiv) was stirred at 25 °C for 0.5 h. The mixture was concentrated under vacuum to give a residue. The residue was purified by prep-HPLC [column, Phenomenex Synergi C18 150 μm × 25 μm × 10 μm; mobile phase, water (0.05% HCl)/acetonitrile; B%, 19% to 39%, 6.5 min] to give **S9-2c** (32.08 mg, 77.2% yield, 97.8% purity) as a yellow solid.

Synthesis of ***S9-3c.*** To a solution of intermediate **4** (100 mg, 199 μmol, 1.00 equiv) and 17-azido-3,6,9,12,15-pentaoxaheptadecyl 4-methylbenzenesulfonate (123 mg, 239 μmol, 1.20 equiv) in DMF (0.500 mL) was added K_2CO_3 (55.1 mg, 398 μmol, 2.00 equiv). The mixture was stirred at 60 °C for 3 h. The reaction mixture was partitioned between water (2.00 mL) and EtOAc (2.00 mL). The water phase was separated and washed with EtOAc (2 × 2.00 mL). The combined organic phase was washed with brine (2 × 2.00 mL), dried over anhydrous Na_2SO_4, filtered, and concentrated under reduced pressure to give a residue. The residue was purified by prep-HPLC [neutral condition; column, Waters Xbridge 150 mm × 25 mm × 5 μm; mobile phase, water (10 mM NH_4HCO_3)/acetonitrile; B%, 40% to 70%, 10 min] to give *tert*-butyl [1-(6-amino-5-{4-[(17-azido-3,6,9,12,15-pentaoxaheptadecyl)oxy]-2,3-dichlorophenyl}-pyrazin-2-yl)-4-methylpiperidin-4-yl]carbamate (66.0 mg, 87.1 μmol, 43.7% yield) as a yellow oil.

To a solution of *tert*-butyl [1-(6-amino-5-{4-[(17-azido-3,6,9,12,15-pentaoxaheptadecyl)oxy]-2,3-dichlorophenyl}-pyrazin-2-yl)-4-methylpiperidin-4-yl]carbamate (66.0 mg, 87.1 μmol, 1.00 equiv) in THF (1.00 mL) was added 10% Pd/C (7.00 mg, 87.1 μmol, 1.00 equiv) under N_2. The suspension was degassed under vacuum and purged with H_2 several times. The mixture was stirred under H_2 (15 psi) at 15 °C for 2 h. The mixture was filtered, and the filtrate was concentrated under reduced pressure to afford *tert*-butyl [1-(6-amino-5-{4-[(17-amino-3,6,9,12,15-pentaoxaheptadecyl)oxy]-2,3-dichlorophenyl}pyrazin-2-yl)-4-methylpiperidin-4-yl]-carbamate (63.0 mg, 86.1 μmol, 98.9% yield) as a brown oil, which was used without further purification.

To a solution of *tert*-butyl [1-(6-amino-5-{4-[(17-amino-3,6,9,12,15-pentaoxaheptadecyl)oxy]-2,3-dichlorophenyl}-pyrazin-2-yl)-4-methylpiperidin-4-yl]carbamate (63.0 mg, 86.1 μmol, 1.00 equiv) and intermediate **2** (49.3 mg, 129 μmol, 1.50 equiv, HCl) in DMF (1.00 mL) were added HATU (39.3 mg, 103 μmol, 1.20 equiv) and DIPEA (50.1 mg, 387 μmol, 67.5 μL, 4.50 equiv). Then the mixture was stirred at 15 °C for 13 h. The residue was purified by prep-HPLC [neutral condition; column, Waters Xbridge 150 mm × 25 mm × 5 μm; mobile phase, water (10 mM NH_4HCO_3)/acetonitrile; B%, 32% to 62%, 10 min] to give *tert*-butyl [1-(6-amino-5-{2,3-dichloro-4-[(1-{[2-(2,6-dioxopiperidin-3-yl)-1,3-dioxoisoindolin-4-yl]oxy}-2-oxo-6,9,12,15,18-pentaoxa-3-azaicosan-20-yl)oxy]phenyl}pyrazin-2-yl)-4-methylpiperidin-4-yl]carbamate (77.0 mg, 73.6 μmol, 85.5% yield) as a yellow solid.

To a solution of compound *tert*-butyl [1-(6-amino-5-{2,3-dichloro-4-[(1-{[2-(2,6-dioxopiperidin-3-yl)-1,3-dioxoisoindolin-4-yl]oxy}-2-oxo-6,9,12,15,18-pentaoxa-3-azaicosan-20-yl)oxy]phenyl}pyrazin-2-yl)-4-methylpiperidin-4-yl]carbamate (77.0 mg, 73.6 μmol, 1.00 equiv) in EtOAc (0.700 mL) was added HCl/EtOAc (4 M, 184 μL, 10.0 equiv), and then the mixture was stirred at 15 °C for 2 h. The mixture was concentrated under reduced pressure to give a residue. The residue was purified by prep-HPLC [HCl condition; column, Phenomenex Synergi C18 150 mm × 30 mm × 4 μm; mobile phase, water (0.05% HCl)/acetonitrile; B%, 6% to 36%, 10 min] to give **S9-3c** (29.5 mg, 29.5 μmol, 40.1% yield, 98.2% purity, HCl) as a yellow solid.

Synthesis of ***S9-4c.*** To a solution of intermediate **5** (100 mg, 197 μmol, 1.00 equiv) and 17-azido-3,6,9,12,15-pentaoxaheptadecyl 4-methylbenzenesulfonate (122 mg, 237 μmol, 1.20 equiv) in DMF (1.00 mL) was added K_2CO_3 (54.5 mg, 395 μmol, 2.00 equiv). The mixture was stirred at 60 °C for 3 h. The reaction mixture was partitioned between water (2.00 mL) and EtOAc (2.00 mL). The water phase was separated and washed with ethyl acetate (2 × 2.00 mL). The combined organic phase was washed with brine (2 × 2.00 mL), dried over anhydrous Na_2SO_4, filtered, and concentrated under reduced pressure to give a residue. The residue was purified by prep-HPLC [neutral

https://doi.org/10.1021/acs.biochem.1c00377
Biochemistry 2021, 60, 2593−2609

Scheme 6

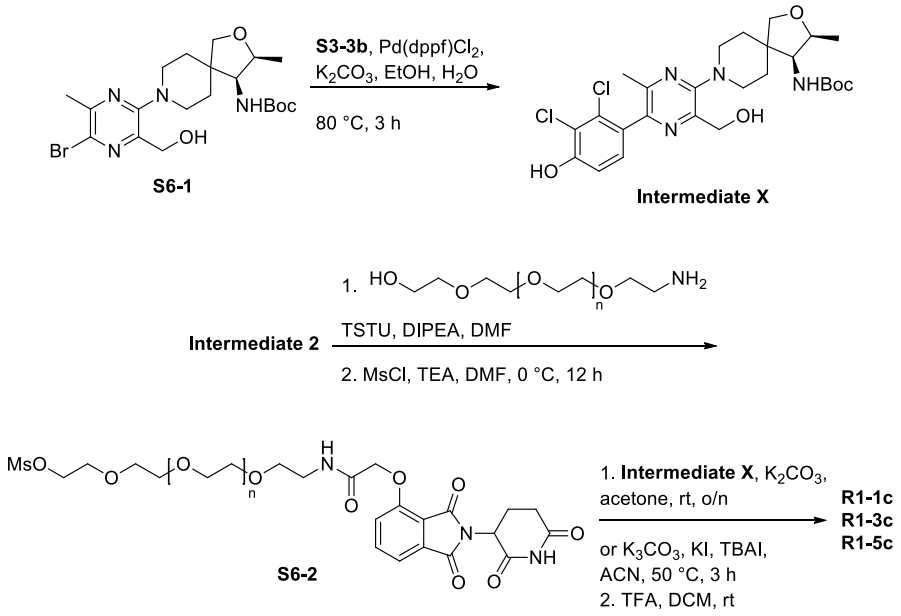

condition; column, Waters Xbridge 150 mm × 25 mm × 5 μm; mobile phase, water (10 mM NH_4HCO_3)/acetonitrile; B%, 44% to 74%, 10 min]. The product *tert*-butyl [1-(6-amino-5-{5-[(17-azido-3,6,9,12,15-pentaoxaheptadecyl)oxy]-2,3-dichlorophenyl}pyrazin-2-yl)-4-methylpiperidin-4-yl]carbamate (79.0 mg, 104 μmol, 52.9% yield) was obtained as a yellow oil.

To a solution of *tert*-butyl [1-(6-amino-5-{5-[(17-azido-3,6,9,12,15-pentaoxaheptadecyl)oxy]-2,3-dichlorophenyl}-pyrazin-2-yl)-4-methylpiperidin-4-yl]carbamate (79.0 mg, 104 μmol, 1.00 equiv) in THF (1.00 mL) was added 10% Pd/C (8.00 mg, 10.4 μmol, 0.100 equiv) under N_2. The suspension was degassed under vacuum and purged with H_2 several times. The mixture was stirred under H_2 (15 psi) at 15 °C for 3 h. The reaction mixture was filtered and concentrated under reduced pressure to give the product *tert*-butyl [1-(6-amino-5-{5-[(17-amino-3,6,9,12,15-pentaoxaheptadecyl)oxy]-2,3-dichlorophenyl}pyrazin-2-yl)-4-methylpiperidin-4-yl]carbamate (80.0 mg, 93.9 μmol, 90.1% yield, 85.9% purity) as a yellow oil.

To a solution of *tert*-butyl [1-(6-amino-5-{5-[(17-amino-3,6,9,12,15-pentaoxaheptadecyl)oxy]-2,3-dichlorophenyl}-pyrazin-2-yl)-4-methylpiperidin-4-yl]carbamate (80.0 mg, 93.9 μmol, 1.00 equiv) and intermediate **2** (53.8 mg, 141 μmol, 1.50 equiv, HCl) in DMF (1.00 mL) were added HATU (42.9 mg, 113 μmol, 1.20 equiv) and DIPEA (54.6 mg, 423 μmol, 73.6 μL, 4.50 equiv). The mixture was stirred at 15 °C for 16 h. The residue was purified by prep-HPLC [neutral condition; column, Phenomenex luna C18 150 mm × 25 mm × 10 μm; mobile phase, water (10 mM NH_4HCO_3)/acetonitrile; B%, 32% to 62%, 10 min]. The product *tert*-butyl [1-(6-amino-5-{2,3-dichloro-5-[(1-{[2-(2,6-dioxopiperidin-3-yl)-1,3-dioxoisoindolin-4-yl]oxy}-2-oxo-6,9,12,15,18-pentaoxa-3-azaicosan-20-yl)oxy]phenyl}pyrazin-2-yl)-4-methylpiperidin-4-yl]carbamate (77.0 mg, 73.6 μmol, 78.4% yield) was obtained as a yellow solid.

To a solution of *tert*-butyl [1-(6-amino-5-{2,3-dichloro-5-[(1-{[2-(2,6-dioxopiperidin-3-yl)-1,3-dioxoisoindolin-4-yl]oxy}-2-oxo-6,9,12,15,18-pentaoxa-3-azaicosan-20-yl)oxy]phenyl}-pyrazin-2-yl)-4-methylpiperidin-4-yl]carbamate (77.0 mg, 73.6 μmol, 1.00 equiv) in EtOAc (1.00 mL) was added HCl/EtOAc (4 M, 184 μL, 10.0 equiv). The mixture was stirred at 15 °C for 2 h. The reaction mixture was filtered and concentrated under reduced pressure to give a residue. The residue was purified by prep-HPLC [HCl condition; column, Phenomenex Synergi C18 150 μm × 25 μm × 10 μm; mobile phase, water (0.05% HCl)/acetonitrile; B%, 23% to 43%, 11 min]. **S9-4c** (33.6 mg, 33.9 μmol, 46.1% yield, 99.1% purity, HCl) was obtained as a yellow solid.

*tert-Butyl {(3S,4S)-8-[5-(2,3-Dichloro-4-hydroxyphenyl)-3-(hydroxymethyl)-6-methylpyrazin-2-yl]-3-methyl-2-oxa-8-azaspiro[4.5]decan-4-yl}carbamate (intermediate **X**).* The mixture of previously reported[18] *tert*-butyl *N*-{(3*S*,4*S*)-8-[5-bromo-3-(hydroxymethyl)-6-methylpyrazin-2-yl]-3-methyl-2-oxa-8-azaspiro[4.5]decan-4-yl}carbamate (480 mg, 1.02 mmol, 1.00 equiv), 2,3-dichloro-4-(4,4,5,5-tetramethyl-1,3,2-dioxaborolan-2-yl)phenol (359 mg, 1.24 mmol, 1.22 equiv), K_2CO_3 (432 mg, 3.13 mmol, 3.07 equiv), and $Pd(dppf)Cl_2$ (97 mg, 0.132 mmol, 0.13 equiv) in EtOH (12 mL) and water (2.4 mL) was stirred for 3 h at 80 °C under a nitrogen atmosphere. The mixture was allowed to cool to room temperature. The reaction was quenched by the addition of water (30 mL). The resulting mixture was extracted with DCM (3 × 30 mL). The combined organic layers were washed with brine (30 mL) and dried over anhydrous Na_2SO_4. After filtration, the filtrate was concentrated under reduced pressure. The residue was purified by silica gel column chromatography and eluted with DCM/MeOH (9/1) to afford *tert*-butyl *N*-{(3*S*,4*S*)-8-[5-(2,3-dichloro-4-hydroxyphenyl)-3-(hydroxymethyl)-6-methylpyrazin-2-yl]-3-methyl-2-oxa-8-azaspiro[4.5]decan-4-yl}carbamate (intermediate **X**, 400 mg, 60%) as a brown solid (Scheme 6).

General Synthesis of S6-2 (exemplified for *n* = 1). To a stirred mixture of intermediate **2** (6.50 g, 19.56 mmol, 1.00 equiv) and TSTU (8.8 g, 29.34 mmol, 1.50 equiv) in DMF (65 mL) was added DIPEA (5.0 g, 39.12 mmol, 2.00 equiv) dropwise at 0 °C under a nitrogen atmosphere. The resulting mixture was stirred overnight at room temperature. The reaction was quenched with water/ice at room temperature. The resulting mixture was extracted with EtOAc (3 × 100 mL). The combined organic layers were washed with brine (100 mL) and dried over anhydrous Na_2SO_4. After filtration, the filtrate

https://doi.org/10.1021/acs.biochem.1c00377
Biochemistry 2021, 60, 2593−2609

was concentrated under reduced pressure. This resulted in 2,5-dioxopyrrolidin-1-yl 2-{[2-(2,6-dioxopiperidin-3-yl)-1,3-dioxoisoindol-4-yl]oxy}acetate (4.0 g, 38%) as a white solid.

To a stirred mixture of 2,5-dioxopyrrolidin-1-yl 2-{[2-(2,6-dioxopiperidin-3-yl)-1,3-dioxoisoindol-4-yl]oxy}acetate (2.00 g, 4.65 mmol, 1.00 equiv) and 2-{2-[2-(2-aminoethoxy)ethoxy]-ethoxy}ethanol (0.90 g, 4.65 mmol, 1.00 equiv) in DMF (20 mL) was added DIEA (1.20 g, 9.27 mmol, 1.99 equiv) dropwise at 0 °C under a nitrogen atmosphere. The resulting mixture was stirred overnight at room temperature. The reaction mixture was purified by reverse-phase flash chromatography [column, C18 silica gel; mobile phase, acetonitrile in water (0.1% formic acid), 0% to 70% gradient in 10 min; detector, UV 254 nm] to give 2-{[2-(2,6-dioxopiperidin-3-yl)-1,3-dioxoisoindol-4-yl]oxy}-*N*-(2-{2-[2-(2-hydroxyethoxy)ethoxy]ethoxy}ethyl)acetamide (1.1 g, 46%) as a light yellow oil.

To a stirred mixture of 2-{[2-(2,6-dioxopiperidin-3-yl)-1,3-dioxoisoindol-4-yl]oxy}-*N*-(2-{2-[2-(2-hydroxyethoxy)-ethoxy]ethoxy}ethyl)acetamide (1.60 g, 0.31 mmol, 1.00 equiv) and TEA (0.96 g, 0.95 mmol, 3.0 equiv) in DMF (16 mL) was added MsCl (0.55 g, 0.46 mmol, 1.51 equiv) dropwise at 0 °C. The resulting mixture was stirred for 12 h at room temperature. The residue was purified by reverse-phase flash chromatography [column, C18 silica gel; mobile phase, acetonitrile in water (0.1% formic acid), 0% to 70% gradient in 40 min; detector, UV 254 nm] to give 2-(2-{2-[2-(2-{[2-(2,6-dioxopiperidin-3-yl)-1,3-dioxoisoindol-4-yl]oxy}acetamido)ethoxy]ethoxy}ethoxy)-ethylmethanesulfonate (**S6-2*n*= 1**, 840 mg, 45%) as a light yellow oil.

General synthesis of R1-1c, R1-3c, and R1-5c (exemplified for R1-1c). To a stirred mixture of intermediate **X** (100 mg, 0.18 mmol, 1.00 equiv) and **S6-2*n*= 1** (106 mg, 0.18 mmol, 1.00 equiv) in acetone (10 mL) was added K_2CO_3 (75 mg, 0.54 mmol, 3.0 equiv) in portions at room temperature under a nitrogen atmosphere. The resulting mixture was stirred overnight at room temperature under a nitrogen atmosphere. The resulting mixture was purified by reverse-phase flash chromatography [column, C18 silica gel; mobile phase, acetonitrile in water (0.1% formic acid), 10% to 80% gradient in 30 min; detector, UV 254 nm]. The collected fraction was lyophilized to afford *tert*-butyl *N*-[(3*S*,4*S*)-8-(5-{2,3-dichloro-4-[2-(2-{2-[2-(2-{[2-(2,6-dioxopiperidin-3-yl)-1,3-dioxoisoindol-4-yl]oxy}acetamido)ethoxy]ethoxy}ethoxy)ethoxy]-phenyl}-3-(hydroxymethyl)-6-methylpyrazin-2-yl)-3-methyl-2-oxa-8-azaspiro[4.5]decan-4-yl]carbamate (84 mg, 22%) as a white solid.

To a stirred mixture of *tert*-butyl *N*-[(3*S*,4*S*)-8-(5-{2,3-dichloro-4-[2-(2-{2-[2-(2-{[2-(2,6-dioxopiperidin-3-yl)-1,3-dioxoisoindol-4-yl]oxy}acetamido)ethoxy]ethoxy}ethoxy)-ethoxy]phenyl}-3-(hydroxymethyl)-6-methylpyrazin-2-yl)-3-methyl-2-oxa-8-azaspiro[4.5]decan-4-yl]carbamate (40 mg, 0.04 mmol, 1.00 equiv) in DCM (4 mL) was added TFA (0.80 mL) in portions at room temperature under a nitrogen atmosphere. The resulting mixture was stirred for 3 h at room temperature under a nitrogen atmosphere. The resulting mixture was concentrated, and the residue was purified by reverse-phase flash chromatography [column, C18 silica gel; mobile phase, acetonitrile in water (0.1% formic acid), 10% to 50% gradient in 30 min; detector, UV 254 nm]. The crude product (40 mg) was purified by prep-HPLC [column, Xselect CSH OBD 30 mm × 150 mm × 5 μm; mobile phase A, water (0.1% formic acid); mobile phase B, acetonitrile; flow rate, 60 mL/min; gradient, 20% to 34% B in 7 min; 220 nm]. The collected fraction was lyophilized to afford **R1-1c** (21 mg, 56%) as a white solid.

NMR Spectroscopy. All ^{1}H NMR spectra were recorded at 600 MHz and 25 °C, and chemical shifts are represented on the δ scale. Residual protium in the NMR solvent (MeOH-d_4, δ 3.31) was used to reference chemical shifts. Data are represented as follows: assignment, chemical shift, integration, multiplicity (s, singlet; d, doublet; t, triplet; m, multiplet), and coupling constant in hertz. All ^{13}C NMR spectra were recorded at 150 MHz and 25 °C, and chemical shifts are represented on the δ scale. The carbon resonances of the NMR solvent (MeOH-d_4, δ 49.15) are used to reference chemical shifts. Full assignment of protons and carbons was completed on the basis of the following two-dimensional NMR spectroscopy experiments: ^{1}H−^{1}H correlation spectroscopy (COSY), ^{1}H−^{13}C heteronuclear single-quantum coherence non-uniform sampling (HSQC-NUS), and ^{1}H−^{13}C heteronuclear multiple-bond connectivity non-uniform sampling (HMBC-NUS) (Tables S2−S9 and Figures S11−S50).

LC-MS. Samples were separated over a Kinetex C18 column with water and 0.1% formic acid (A) and acetonitrile and 0.1% formic acid (B) as mobile phases. After an initial equilibration period of 3 min at 5% B, a linear gradient to 100% was run over 13 min. The LC stream was inline with an Agilent 6530 qTOF instrument with standard parameters (Table S10 and Figures S51−S57).

Antibodies and Compounds. Antibodies used in this study were obtained commercially from the following sources: SHP2 (Bethyl, catalog no. A301-544A), phospho-Thr202/Tyr204-Erk1/2 (CST, catalog no. 9101), Cereblon (CST, catalog no. 71810), β-actin (Millipore-Sigma, catalog no. A1978), β-tubulin (CST, catalog no. 2146), and GAPDH (CST, catalog no. 5174). SHP099 and RMC-4550 were purchased from DC chemicals (catalog no. DC9737) and ProbeChem Biochemicals (catalog no. PC-35116), respectively. 6,8-Difluoro-4-methylumbelliferyl phosphate (DiFMUP, catalog no. D22065) and 6,8-difluoro-7-hydroxy-4-methylcoumarin (DiFMU, catalog no. D6566) were purchased from Life Technologies.

Cell Culture. The MV-4-11 cell line was purchased from the American Type Culture Collection (ATCC). The KYSE-520 and MOLM-13 cell lines were purchased from DSMZ (Braunschweig, Germany). Parental and CRBN knockout MOLT4 cells were a gift from N. Gray (Dana-Farber Cancer Institute). All cell lines were cultured in RPMI-1640 medium containing 10% FBS and 1% penicillin/streptomycin at 37 °C with 5% CO_2.

Immunoblotting Analysis. Cells were treated with PROTAC compounds as indicated and lysed in RIPA lysis buffer [25 mM Tris-HCl (pH 7.6), 150 mM NaCl, 1% Nonidet P-40, 1% sodium deoxycholate, 0.1% sodium dodecyl sulfate, and 2 mM EDTA] with protease inhibitors (cOmplete Mini, Roche). Lysates were resolved on sodium dodecyl sulfate−polyacrylamide gel electrophoresis gels (Novex Tris-Glycine, ThermoFisher Scientific) and transferred to PVDF membranes using the XCell II wet blotting system (ThermoFisher Scientific). Membranes were blocked with 5% BSA diluted in TBST (Tris-buffered saline and 0.1% Tween 20) buffer and incubated with primary antibodies overnight. The blots were rinsed three times for 10 min each in 15 mL of TBST buffer and incubated with secondary antibodies diluted with 5% BSA for 1 h followed by three final washes. Specific protein bands were

https://doi.org/10.1021/acs.biochem.1c00377
Biochemistry 2021, 60, 2593−2609

Table 1

target	forward primer sequence	reverse primer sequence
DUSP6 set A	CAGCGACTGGAACGAGAATAC	GAACTCGGCTTGGAACTTACT
DUSP6 set B[26]	AGCAGCGACTGGAACGAGAA	TGTTGGACAGCGGACTACCAT
GAPDH	CTTCACCACCATGGAGGAGGC	GGCATGGACTGTGGTCATGAG
β-actin	CAACCGCGAGAAGATGACC	AGCCTGGATAGCAACGTACA

detected using SuperSignal West Pico PLUS Chemiluminescent Substrate (ThermoFisher Scientific).

Measurement of the Inhibitory Activity of Compounds using DiFMUP. The phosphatase activities of SHP2-F285S and the isolated PTP domain were measured using the fluorogenic small molecule substrate DiFMUP. Compounds were dissolved in DMSO at a concentration of 10 mM, diluted 1/10 in assay buffer [60 mM Hepes (pH 7.2), 75 mM KCl, 75 mM NaCl, 1 mM EDTA, 0.05% Tween 20, and 2 mM DTT], and added to 96-well plates in a 3-fold dilution (concentration range from 200 mM to 3.3 nM) in triplicate. The serially diluted compound was mixed with 0.5 nM SHP2-F285S mutant or isolated PTP domain proteins and incubated at room temperature for 1 h, after which 400 mM DiFMUP was added to each well. One hour after the addition of DiFMUP, fluorescence was measured on a SpectraMax M5 plate reader (Molecular Devices) using excitation and emission wavelengths of 340 and 450 nm, respectively, and the inhibitor dose−response curves were analyzed using nonlinear regression curve fitting with control-based normalization.

Cell Viability Analysis. MV-4-11 cells were seeded at a density of 1000 cells/mL of medium in 10 cm plates in triplicate and treated with 100 nM **R1-5C**, 100 nM **R1-1C**, and 100 nM RMC-4550 or DMSO carrier. The cells were replenished with compounds every 24 h and counted on days 1−9 using an automated cell counter (Bio-Rad). KYSE-520 cells were plated onto 96-well plates (500 cells per well) in 100 mL of medium and treated with 100 nM **R1-5C** and 100 nM RMC-4550 or DMSO carrier. The cells were replenished with compounds every 24 h, and cell viability was assessed on days 1, 3, 5, 7, and 9 upon addition of 20 mL of CellTiter-Blue reagent (Promega) to wells and measurement of the luminescent signal using a GloMax discover microplate reader (Promega).

TMT-Based LC-MS3 Proteomics. MV-4-11 cells (10 M) were treated with DMSO carrier or 100 nM **R1-5C**, 100 nM **R1-3C**, 100 nM **R1-1C**, 100 nM RMC-4550, and 1 mM pomalidomide in biological duplicate or singlicate for the indicated time periods. MOLT4 cells (5 M) were treated with 1 mM **R1-5C** for 5 h in biological singlicate. Cells were then harvested by centrifugation, and cell pellets snap-frozen in liquid nitrogen. Sample preparation for TMT LC-MS3 mass spectrometry was performed as described previously.[19]

Expression and Purification of Wild-Type SHP2, F285S-SHP2, and the Isolated PTP Domain. Human wild-type SHP2 (amino acids 1−525, UniProtKB Q06124) was inserted into a modified pGEX6P1 vector with an N-terminal GST tag, followed by a PreScission cleavage site. Recombinant GST-SHP2 protein was overexpressed in *Escherichia coli* BL21 (DE3) cells induced by 0.2 mM isopropyl 1-thio-D-galactopyranoside (IPTG) at 16 °C overnight. Cells were harvested by centrifugation, resuspended in lysis buffer [25 mM Tris 7.5, 150 mM NaCl, 2 mM $MgCl_2$, 2 mM TCEP, and an EDTA-free protease inhibitor cocktail tablet (cOmplete, Roche)], and lysed by sonication. After centrifugation, recombinant GST-SHP2 in supernatant was affinity-purified by Pierce glutathione agarose (Thermo Fisher Scientific) and eluted with lysis buffer containing 20 mM GSH. After GST tag cleavage with the recombinant HRV 3C protease, the SHP2 protein was further purified by a HiTrap Heparin HP column (GE Healthcare). SHP2-containing fractions were pooled and finally polished over a Superdex200 10/300 GL size exclusion column (GE Healthcare) in a buffer containing 25 mM Tris 7.5, 100 mM NaCl, 2 mM $MgCl_2$, and 2 mM TCEP. The protein sample concentration was determined on the basis of the UV absorbance at 280 nm. Wild-type SHP2 protein was concentrated to 18 mg/mL for crystallization. SHP2-F285S and isolated PTP domain proteins were expressed and purified as described previously.[8]

Crystallization and Structure Determination. The hanging-drop vapor diffusion method was used for co-crystallization of wild-type SHP2 in complex with RMC-4550. Wild-type SHP2 was incubated with RMC-4550 at a molar ratio of 1/2, and crystals were grown at 18 °C by mixing equal volumes of the protein sample and reservoir solution [0.1 M sodium chloride, 0.1 M Bis-Tris propane (pH 8.5), and 11% PEG 1500]. Diffraction quality crystals were cryoprotected by supplementing a reservoir solution with 20% glycerol and flash-frozen in liquid nitrogen. X-ray diffraction data were collected at Advanced Photon Source NE-CAT beamline 24 ID-E at 100 K using a wavelength of 0.979 Å. The diffraction images from single crystals were processed and scaled using XDS.[20] To obtain phases, molecular replacement for both copies of SHP2 in the unit cell was performed in Phenix with Phaser using chain B of a SHP2 crystal structure [Protein Data Bank (PDB) entry 5EHR] as the search model. Iterative model building was performed in COOT.[21] Reciprocal space refinement was performed in phenix.refine, using reciprocal space optimization of xyz coordinates, individual atomic *B*-factors, NCS restraints, optimization for X-ray/stereochemistry weights, and optimization for X-ray/ADP weights.[22] The RMC-4550 ligand coordinate and restraint file were generated using eLBOW.[23] In the final cycles of model building, NCS restraints were removed during refinement and overall model quality was assessed using MolProbity.[24] All crystallographic data processing, refinement, and analysis software was compiled and supported by the SBGrid Consortium.[25]

Real-Time Quantitative Polymerase Chain Reaction (qPCR). One million cells were treated with **R1-5C** at 200 nM or DMSO for 2 or 16 h. Cells were harvested after treatment in TRIzol (Thermo Fisher), and RNA was purified by phenol/chloroform extraction using MaXtract high-density tubes (Qiagen). RNA was treated with Turbo DNase (Thermo Fisher) for 30 min at 37 °C and then re-extracted with chloroform isoamyl alcohol using MaXtract high-density tubes; 1 μg of RNA for each sample was used to make cDNA using the iScript cDNA synthesis kit (Bio-Rad). qPCR was performed using PowerUp SYBR Green Master Mix (Thermo Fisher) in a 10 μL total reaction volume with 0.25 μM forward and reverse

https://doi.org/10.1021/acs.biochem.1c00377
Biochemistry 2021, 60, 2593−2609

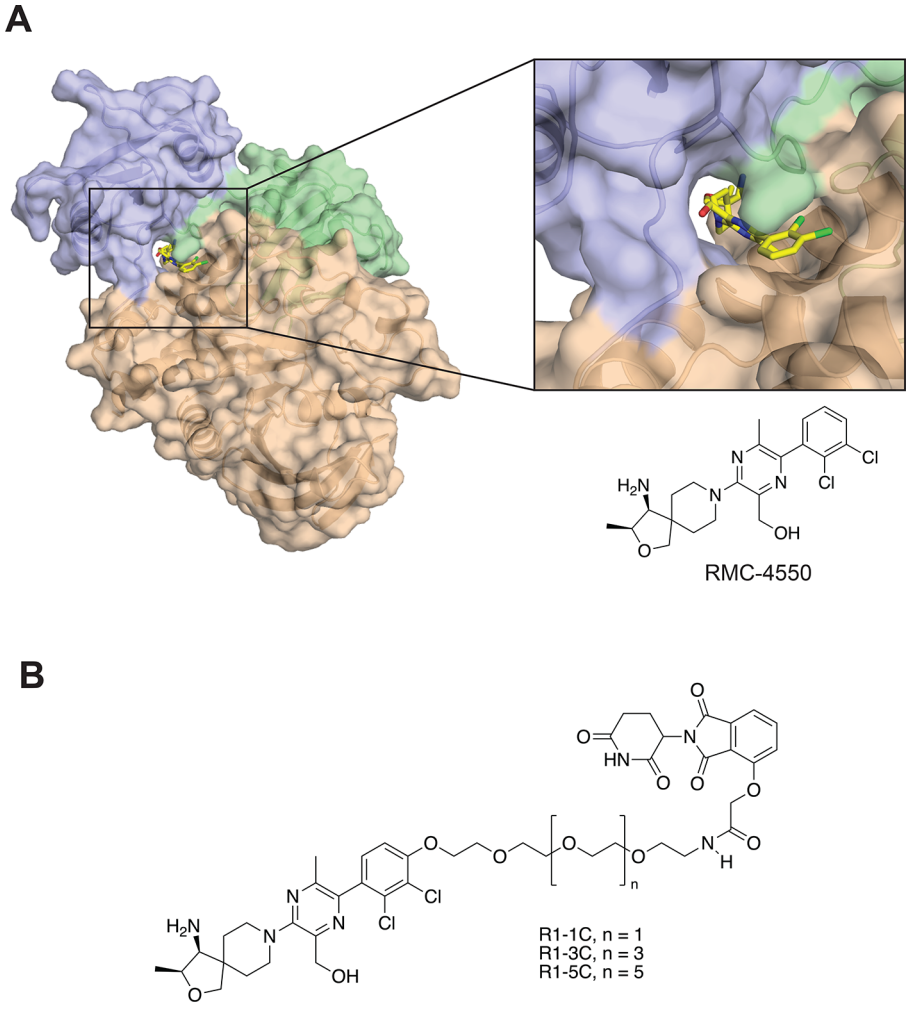

Figure 1. Structure of SHP2 protein in complex with RMC-4550. (A) Chemical structure of RMC-4550 and X-ray crystal structure of SHP2 in complex with RMC-4550 (PDB entry 7RCT). Surface representation of SHP2 in complex with RMC-4550 bound in the central tunnel formed at the interface of the N-SH2 (green), C-SH2 (blue), and PTP (wheat) domains. (B) Chemical structures of RMC-4550-based PROTAC candidates **R1-1C**, **R1-3C**, and **R1-5C**.

primers, with two technical replicates per experiment. Primer sequences are listed in Table 1. Expression was normalized to the average of GAPDH and β-actin expression. Significant differences were identified using Welch's t test in PRISM 9.0.2.

RESULTS

The CRBN E3 ligase ligands (pomalidomide, lenalidomide, and thalidomide, collectively termed IMiDs) have been successfully employed in the design of a wide range of PROTACs to degrade various proteins.[27−30] To develop an effective SHP2 PROTAC, therefore, we first designed a series of compounds designed to tether SHP099 to the IMiD pomalidomide.

To guide the sites for attachment of the linker to the SHP099 warhead, we relied on the X-ray structure of the SHP2-SHP099 complex (PDB entry 5EHR), which shows that there is an exit path for the linker when coupled at either of two positions on the dichloro-substituted aromatic ring (Figure S1A). Two different linker strategies were therefore employed, using either aliphatic or ether attachments to the SHP099 warhead (Figure S1B−E).

We tested whether any of these compounds catalyzed degradation of SHP2 in the MV4;11 acute myeloid leukemia cell line. When MV4;11 cells were treated with these compounds at doses ranging from 0.01 to 50 μM, there was no evidence of SHP2 degradation for any of the compounds, as judged by a Western blot (Figure S2A).

Because none of these first-generation compounds resulted in SHP2 degradation, we determined whether the conjugation of pomalidomide to the SHP099 warhead affected the inhibitory potency of the parent SHP099 compound. We compared the inhibitory activity of SHP099 with the various SHP099-pomalidomide conjugates in enzymatic assays with purified protein, using the fluorogenic substrate DiFMUP and the weakly active SHP2 mutant F285S. Upon titration of SHP099, the F285S enzyme showed a dose-dependent inhibition of phosphatase activity with a half-maximal inhibitory concentration (IC_{50}) of 62 nM, similar to our previous findings[31] for its IC_{50}, and similar to the K_D values for wild-type SHP2.[4] In contrast, the inhibitory profiles of the SHP099-IMiD conjugates are right-shifted, with IC_{50} values ranging from 0.5 to 3.7 μM (Figure S2B), indicating that the coupling of the linker to the warhead reduces the inhibitory potency between roughly 10- and 100-fold, depending on the site of attachment and the nature of the linkage. In fact, simply installing a PEG chain on SHP099 caused a 10-fold decrease in inhibitory activity *in vitro* and in cells (Figure S3A−C). Together, these findings revealed that coupling the linker to the warhead results in a minimum

https://doi.org/10.1021/acs.biochem.1c00377
Biochemistry 2021, 60, 2593−2609

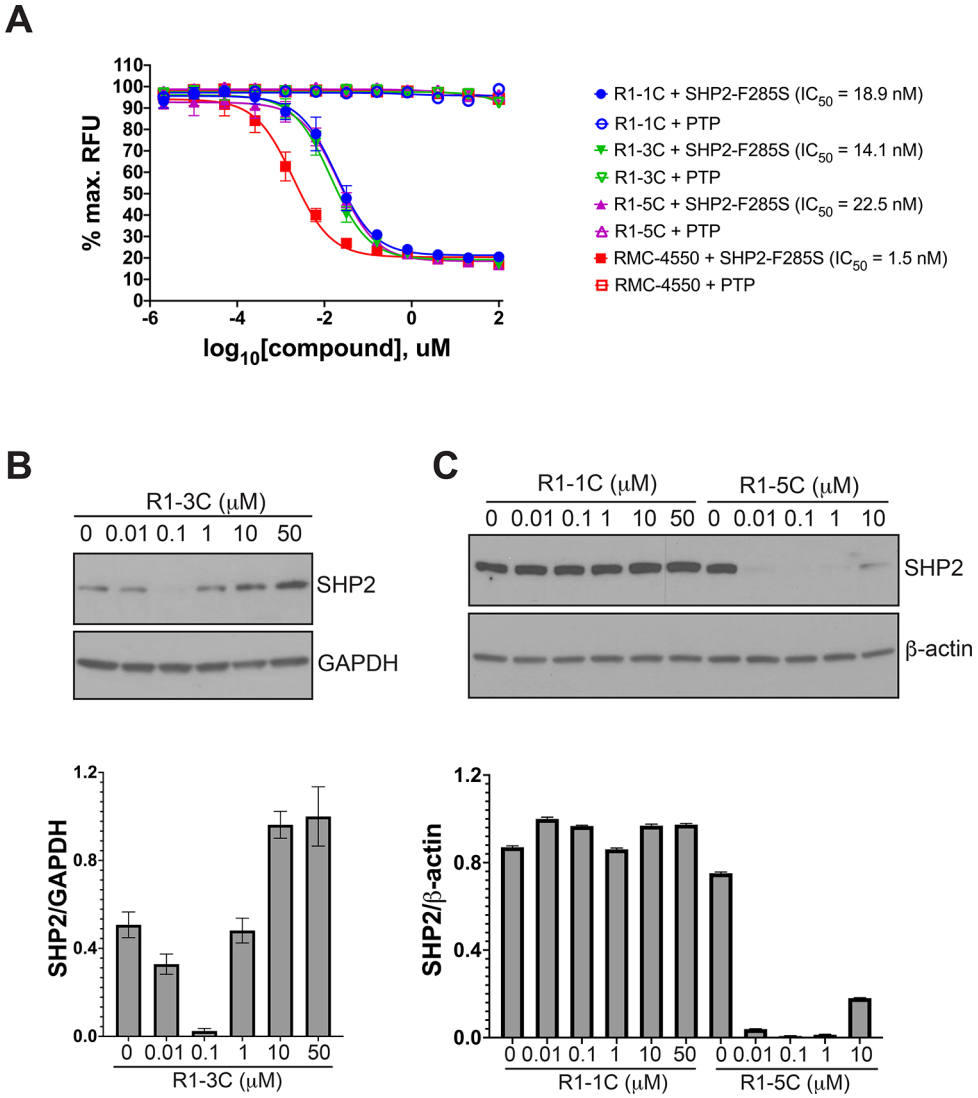

Figure 2. SHP2 degradation induced by RMC-4550-based PROTACs. (A) Inhibition of SHP2-F285S- or PTP-mediated DIFMUP dephosphorylation by **R1-1C**, **R1-3C**, **R1-5C**, and RMC-4550. MV4;11 cells were treated with increasing doses of (B) **R1-3C** or (C) **R1-1C** or (C) **R1-5C** for 24 h and subjected to Western blotting using SHP2, GAPDH, and β-actin antibodies. Quantification of band intensities on the gels is shown below the blots.

~10-fold reduction in potency and suggested that an active PROTAC would require a more potent warhead to offset this consequence of linker coupling.

RMC-4550 is an allosteric inhibitor of SHP2 (Figure 1A) with a potency that is 50-fold higher than that of SHP099 *in vitro*.[12] To determine whether a similar exit path for the linker exists for RMC-4550 bound to SHP2, we determined the structure of RMC-4550 bound to wild-type SHP2 by X-ray crystallography to 1.8 Å resolution (Figure 1A and Table S1). The structure shows that the dichlorophenyl ring of RMC-4550 adopts a pose virtually identical to that of SHP099 when bound, exposing the same tethering sites to solvent for the design of PROTAC compounds (Figure S4A,B).

Because **S9-3C** is the most potent of all SHP099-IMiD conjugates, we substituted SHP099 with RMC-4550 in this design to create **R1-3C** (Figure 1B). Upon titration of **R1-3C**, the SHP2 mutant F285S showed a dose-dependent inhibition of phosphatase activity with an IC_{50} of 14 nM (Figure 2A), a roughly 10-fold reduction compared to that of RMC-4550 (IC_{50} = 1.5 nM). As expected, this compound displayed no inhibitory activity toward the free catalytic domain (PTP).

We treated MV4;11 cells with increasing doses of **R1-3C** or with DMSO carrier as a control for 24 h and measured SHP2 protein levels by Western blotting. We observed a dose-dependent decrease in SHP2 levels with maximal degradation at 100 nM (Figure 2B). The loss of activity observed at higher **R1-3C** concentrations (1, 10, and 50 μM), termed a hook effect, is a signature trait of PROTACs. The increase in the amount of SHP2 protein upon treatment of MV4;11 cells with high concentrations of **R1-3C** is consistent with the hook effect, in which SHP2 and CRBN are bound to different PROTAC molecules. It may be that allosteric inhibition of SHP2 extends its half-life, that inhibition of CRBN generally affects protein turnover, or that a combination of these two mechanisms contribute.

Because the length of the linker plays a key role in the potency of PROTACs,[32−35] we varied the linker lengths between RMC-4550 and pomalidomide to search for a PROTAC with higher potency. Extension of the linker with two additional PEG units

https://doi.org/10.1021/acs.biochem.1c00377
Biochemistry 2021, 60, 2593−2609

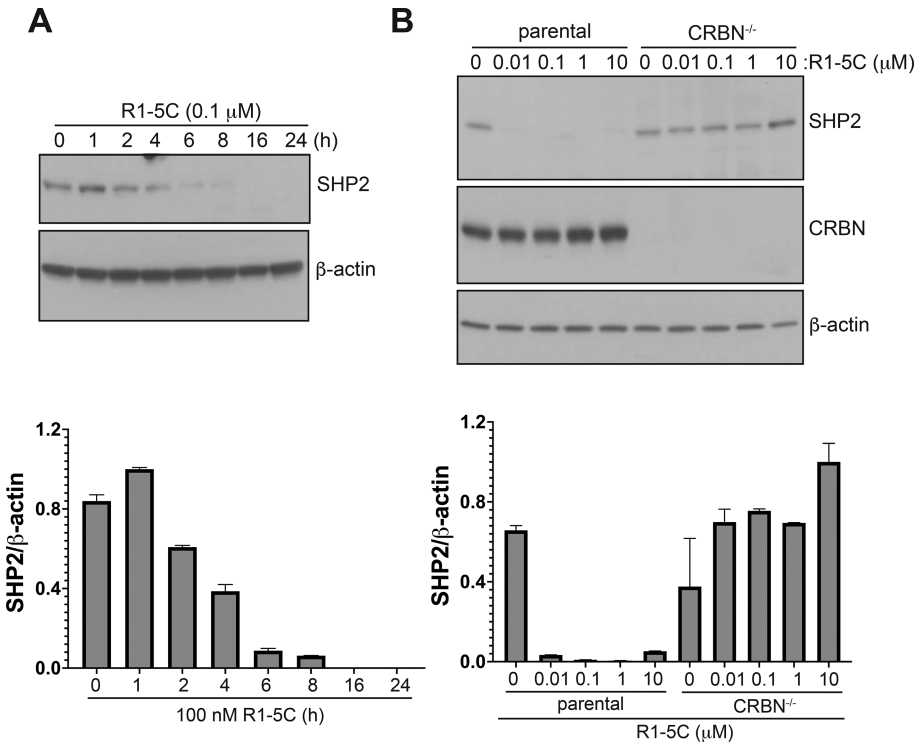

Figure 3. Cell-based evaluation of **R1-5C**. (A) Time course of SHP2 degradation by **R1-5C** (100 nM) in MV4;11 cells. Immunoblotting with SHP2 and β-actin antibodies. (B) CRBN$^{-/-}$ and parental MOLT4 cells were treated with increasing doses of **R1-5C** for 24 h and subjected to Western blotting using SHP2, CRBN, and β-actin antibodies. Quantification of band intensities on the gels is shown below the blots.

(**R1-5C** in Figures 1B, 2C, and S5A) resulted in a PROTAC with greater potency, whereas shortening the linker by two PEG units (**R1-1C** in Figures 1B and 2C) caused complete loss of PROTAC activity.

To determine the kinetics of R1-5C-mediated degradation of SHP2 in MV4;11 cells, we assessed the abundance of SHP2 protein at a series of time points after addition of the compound. SHP2 levels are substantially reduced within 6 h of **R1-5C** treatment, reaching maximal depletion after 16 h (Figure 3A). SHP2 remains depleted at 24 h; however, it reaccumulates to pretreatment levels by 48 h (Figure S5B), consistent with cellular half-lives observed for other PROTACs.[27] The increase in the amount of SHP2 protein 4−6 days after the initial PROTAC treatment likely results from induction of new SHP2 synthesis as a compensatory cellular response to SHP2 depletion.

We confirmed the dependence of SHP2 depletion on the CRBN E3 ligase by comparing the degradation activity of our PROTAC compounds in parental MOLT4 and CRBN$^{-/-}$ knockout cells. Whereas PROTAC treatment decreased the abundance of SHP2 protein in MOLT4 parental cells, PROTAC-dependent degradation of SHP2 was not detectable in CRBN$^{-/-}$ cells, confirming the CRBN requirement for PROTAC activity (Figures 3B and S5C).

We then performed time-resolved quantitative proteomics to further evaluate the selectivity of these compounds for SHP2 and to determine the kinetics of SHP2 degradation in MV4;11 cells. The cells were treated with **R1-5C** (100 nM for 2, 4, 8, or 16 h), **R1-3C** (100 nM for 4 or 16 h), **R1-1C** (100 nM for 4 or 16 h), RMC-4550 (100 nM for 16 h), pomalidomide (1 μM for 5 h), or a vehicle control (DMSO), and the abundance of protein was measured quantiatively using 16-plex tandem mass tag (TMT) isobaric labels, as described previously.[19] **R1-5C** exhibits a striking specificity for degradation of SHP2, which is evident within 4 h (Figure 4). At 16 h, many of the secondary effects of SHP2 depletion recapitulate the consequence of allosteric inhibition (proteins labeled in blue in panels C and D of Figure 4 highlighted with yellow dots in Figure S6), providing further evidence of the SHP2 specificity of the **R1-5C** PROTAC. By comparison, **R1-3C**, which has a shorter linker, resulted in more moderate SHP2 depletion at 16 h (Figure S7A), and **R1-1C** did not induce SHP2 degradation even at 16 h, as anticipated (Figure S7B). Pomalidomide-induced degradation of classical IMiD targets (IKZF1 and ZFP91) serves as a positive control and validates the authenticity of the proteomics experiment (Figures 4E and S7C). Quantitative proteomics of MOLT4 cells treated with **R1-5C** compared to the DMSO control after 5 h also showed that SHP2 is the only protein with a significantly reduced abundance in MOLT4 cells (Figure S8).

To assess the time-dependent recovery of the abundance of SHP2 protein, we treated MV4;11 cells with 100 nM **R1-5C** for 24 h, washed out the compound, and lysed cells at various time points after washout for immunoblotting. The abundance of SHP2 protein recovered to basal (DMSO-treated) levels 24 h after washout (Figure S9).

We also examined whether **R1-5C** affects MAPK signaling. We treated KYSE-520 cells with **R1-5C** or DMSO carrier and monitored the levels of the DUSP6 transcript, a commonly used pharmacodynamic marker for MAPK pathway activity downstream of SHP2.[4] Cells treated with **R1-5C** showed significant downregulation of the amounts of DUSP6 mRNA (Figures 5A and S10). Suppression of the abundance of the DUSP6 transcript is observed both after treatment for 2 and 16 h; the reduction at the late time point reports on the effect of SHP2 degradation on the amounts of DUSP6 mRNA, whereas the reduction at the 2 h time point indicates that allosteric inhibition

https://doi.org/10.1021/acs.biochem.1c00377
Biochemistry 2021, 60, 2593−2609

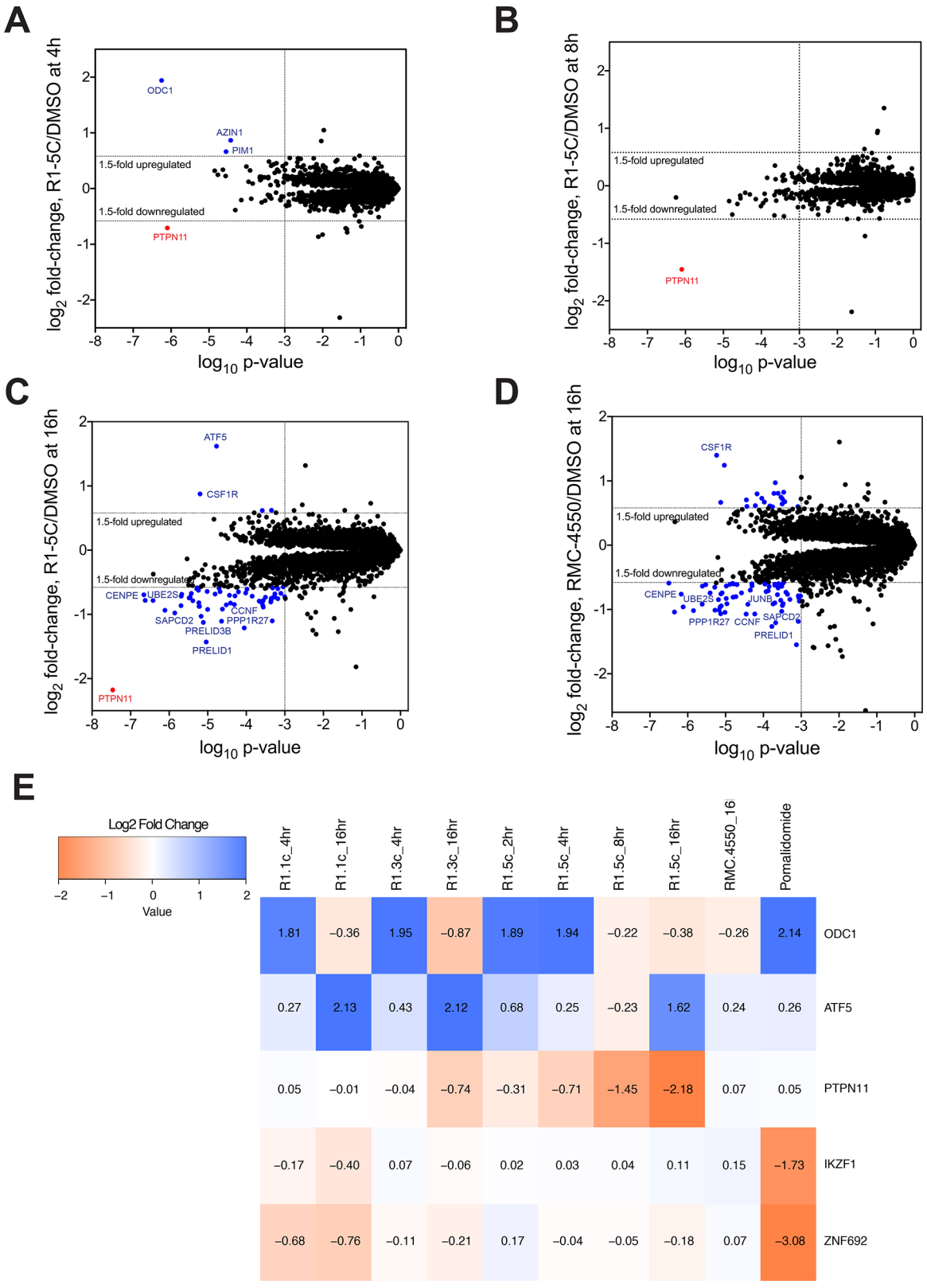

Figure 4. Proteomics analysis showing selective SHP2 degradation by **R1-5C**. (A–D) Scatter plots displaying the relative fold change in the abundance of SHP2 following treatment of MV4;11 cells with 100 nM **R1-5C** for (A) 4 h, (B) 8 h, or (C) 16 h or (D) 100 nM RMC-4550. SHP2/PTPN11 is colored red. Hits colored blue in panels C and D indicate changes in the abundance of proteins at the 16 h time point due to secondary effects (such as transcriptional responses) of SHP2 degradation or inhibition. (E) Heat map of the changes in the abundance of protein in MV4;11 cells comparing treatment with 100 nM **R1-1C** (4 and 16 h), 100 nM **R1-3C** (4 and 16 h), 100 nM **R1-5C** (2, 4, 8, and 16 h), 100 nM RMC-4550 (16 h), and 1 μM pomalidomide (5 h). The heat map colors are scaled with red indicating a decrease in the abundance of protein (−2 $\log_2$ FC) and blue indicating an increase (2 $\log_2$ FC).

https://doi.org/10.1021/acs.biochem.1c00377
Biochemistry 2021, 60, 2593−2609

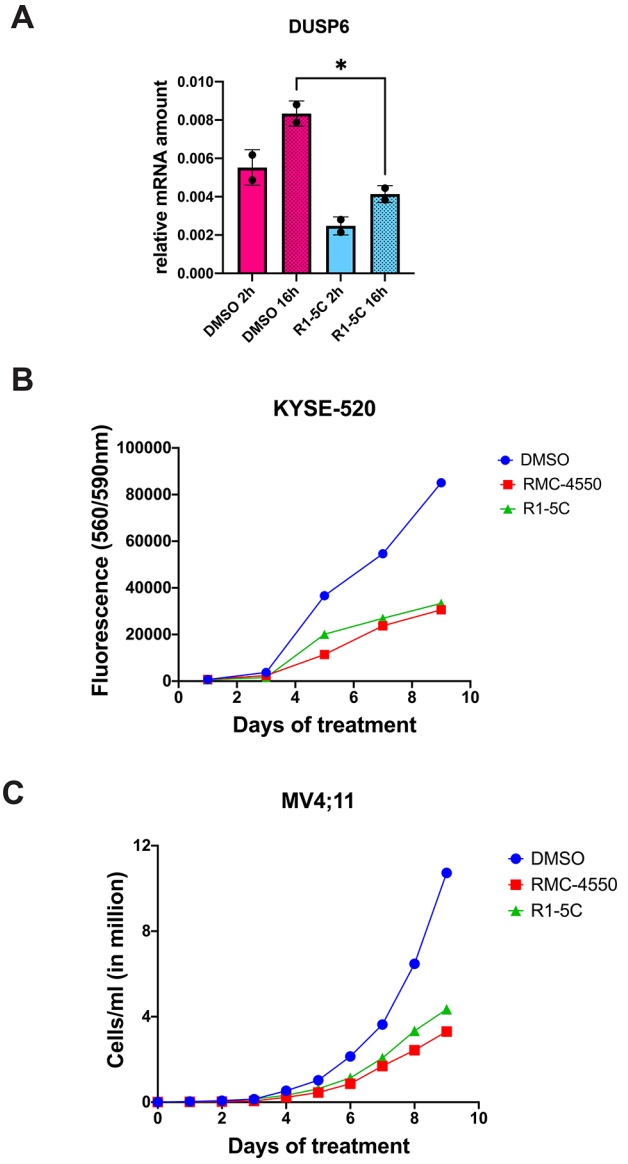

Figure 5. R1-5C inhibits MAPK signaling and suppresses cancer cell growth. (A) Downregulation of DUSP6 transcript levels in KYSE-520 cells after treatment for 2 and 16 h with 200 nM **R1-5C** or DMSO carrier. DUSP6 mRNA was quantified by RT-qPCR using primer set B. (B and C) Cells were treated with 100 nM **R1-5C**, 100 nM RMC-4550, or DMSO carrier in triplicate, and cell numbers were assessed at the indicated time points by automated cell counting (for MV4;11 cells) or the CellTiter-Blue assay (for KYSE-520 cells).

of SHP2 by the RMC-4550 warhead is ongoing prior to SHP2 depletion. The inhibition of cancer cells by **R1-5C** was also assessed in a cell proliferation assay, which showed that **R1-5C** significantly inhibits KYSE-520 and MV4;11 cell growth, with an inhibitory effect comparable to that of RMC-4550 (Figure 5B,C).

DISCUSSION

We report here the design and evaluation of **R1-5C**, a potent and highly selective SHP2 PROTAC featuring an SHP2 allosteric site-binding warhead and the CRBN-targeting IMiD pomalidomide. **R1-5C** expands the range of PROTACs targeting SHP2, which currently include a VHL-targeting PROTAC[36] and the Novartis clinical candidate TNO155 coupled to thalidomide.[37]

Key features required for the degradative activity of our designed compound include the warhead coupling site, the linker chemistry, and the linker length. The high degree of selectivity of **R1-5C** for SHP2 has been documented in this study using stringent whole proteome analysis in two different cell lines, MV4;11 (Figure 4) and MOLT4 (Figure S8). In both of these lines, SHP2 (gene name PTPN11) is the only protein that shows a statistically significant reduction in abundance at time points from 4 to 8 h, before secondary effects of SHP2 inhibition can be observed. By comparison, the selectivity of other reported SHP2-targeting PROTACS has not yet been assessed using whole proteomic studies.[36,37]

Whereas some IMiD-dependent PROTACs can induce detectable degradation of target proteins within 0.5 h, treatment with **R1-5C** for several hours is required before significant depletion of SHP2 is observed in either cell line. Although the origin of the slower onset of SHP2 degradation is not clear, the other recently reported, SHP2-targeting PROTACs also exhibit similar degradation kinetics based on Western blot analysis, independent of whether degradation is mediated by VHL[36] or CRBN.[37]

R1-5C and related compounds are poised to serve as useful tools for the investigation of the physiological roles of SHP2. An important question to be addressed in future work is whether **R1-5C** can be optimized to power degradation of oncogenic, mutant forms of SHP2. Such SHP2 PROTACs would then extend compound efficacy beyond RTK- and ERK-dependent cancers that harbor wild-type SHP2 to cancers with mutant SHP2 and to patients with human genetic disorders like Noonan and LEOPARD syndromes.

ASSOCIATED CONTENT

Supporting Information

The Supporting Information is available free of charge at https://pubs.acs.org/doi/10.1021/acs.biochem.1c00377.

Figures S1−S57 and Tables S1−S10 (PDF)

Accession Codes

Diffraction data and refined coordinates for the SHP2-RMC4550 complex have been deposited as Protein Data Bank entry 7RCT. UNIPROT accession IDs for proteins SHP2, Q06124; ERK1, P27361; ERK2, P28482; PD-1, Q15116; CRBN, Q96SW2; β-actin, P60709; β-tubulin, P07437; GAPDH, P04406; DUSP6, Q16828; IKZF1, Q13422; ZFP91, Q96JP5; VHL, P40337.

AUTHOR INFORMATION

Corresponding Author

Stephen C. Blacklow − *Department of Biological Chemistry and Molecular Pharmacology, Harvard Medical School, Boston, Massachusetts 02115, United States; Department of Cancer Biology, Dana-Farber Cancer Institute, Boston, Massachusetts 02215, United States;* orcid.org/0000-0002-6904-1981; Email: Stephen_blacklow@hms.harvard.edu

Authors

Vidyasiri Vemulapalli − *Department of Biological Chemistry and Molecular Pharmacology, Harvard Medical School, Boston, Massachusetts 02115, United States; Department of Cancer Biology, Dana-Farber Cancer Institute, Boston, Massachusetts 02215, United States;* orcid.org/0000-0002-3368-4766

https://doi.org/10.1021/acs.biochem.1c00377
Biochemistry 2021, 60, 2593−2609

Katherine A. Donovan − *Department of Cancer Biology, Dana-Farber Cancer Institute, Boston, Massachusetts 02215, United States;* orcid.org/0000-0002-8539-5106
Tom C. M. Seegar − *Department of Molecular Genetics, Biochemistry and Microbiology, University of Cincinnati College of Medicine, Cincinnati, Ohio 45267, United States*
Julia M. Rogers − *Department of Biological Chemistry and Molecular Pharmacology, Harvard Medical School, Boston, Massachusetts 02115, United States*
Munhyung Bae − *Department of Biological Chemistry and Molecular Pharmacology, Harvard Medical School, Boston, Massachusetts 02115, United States*
Ryan J. Lumpkin − *Department of Cancer Biology, Dana-Farber Cancer Institute, Boston, Massachusetts 02215, United States*
Ruili Cao − *Department of Biological Chemistry and Molecular Pharmacology, Harvard Medical School, Boston, Massachusetts 02115, United States*
Matthew T. Henke − *Department of Biological Chemistry and Molecular Pharmacology, Harvard Medical School, Boston, Massachusetts 02115, United States*
Soumya S. Ray − *RA Capital, Boston, Massachusetts 02116, United States*
Eric S. Fischer − *Department of Biological Chemistry and Molecular Pharmacology, Harvard Medical School, Boston, Massachusetts 02115, United States; Department of Cancer Biology, Dana-Farber Cancer Institute, Boston, Massachusetts 02215, United States;* orcid.org/0000-0001-7337-6306
Gregory D. Cuny − *Department of Pharmacological and Pharmaceutical Sciences, University of Houston, Houston, Texas 77204, United States;* orcid.org/0000-0002-3188-4748

Complete contact information is available at: https://pubs.acs.org/10.1021/acs.biochem.1c00377

Funding

This work was supported by The Quadrangle Fund for Advancing and Seeding Translational Research at Harvard Medical School (S.C.B.) and National Institutes of Health Grant R35 CA220340 (S.C.B.).

Notes

The authors declare the following competing financial interest(s): S.C.B. is a member of the SAB of Erasca, Inc., is an advisor to MPM Capital, and is a consultant on unrelated projects for IFM, Odyssey Therapeutics, Scorpion Therapeutics, and Ayala Therapeutics. S.R. is an entrepreneur in residence at RA Capital.

■ ACKNOWLEDGMENTS

The authors thank Jon Aster and members of the Blacklow laboratory for helpful discussions.

■ REFERENCES

(1) Bentires-Alj, M.; Paez, J. G.; David, F. S.; Keilhack, H.; Halmos, B.; Naoki, K.; Maris, J. M.; Richardson, A.; Bardelli, A.; Sugarbaker, D. J.; Richards, W. G.; Du, J.; Girard, L.; Minna, J. D.; Loh, M. L.; Fisher, D. E.; Velculescu, V. E.; Vogelstein, B.; Meyerson, M.; Sellers, W. R.; Neel, B. G. Activating mutations of the noonan syndrome-associated SHP2/PTPN11 gene in human solid tumors and adult acute myelogenous leukemia. *Cancer Res.* **2004**, *64*, 8816−8820.
(2) Tartaglia, M.; Niemeyer, C. M.; Fragale, A.; Song, X.; Buechner, J.; Jung, A.; Hahlen, K.; Hasle, H.; Licht, J. D.; Gelb, B. D. Somatic mutations in PTPN11 in juvenile myelomonocytic leukemia, myelodysplastic syndromes and acute myeloid leukemia. *Nat. Genet.* **2003**, *34*, 148−150.
(3) Darian, E.; Guvench, O.; Yu, B.; Qu, C. K.; MacKerell, A. D., Jr. Structural mechanism associated with domain opening in gain-of-function mutations in SHP2 phosphatase. *Proteins: Struct., Funct., Genet.* **2011**, *79*, 1573−1588.
(4) Chen, Y. N.; LaMarche, M. J.; Chan, H. M.; Fekkes, P.; Garcia-Fortanet, J.; Acker, M. G.; Antonakos, B.; Chen, C. H.; Chen, Z.; Cooke, V. G.; Dobson, J. R.; Deng, Z.; Fei, F.; Firestone, B.; Fodor, M.; Fridrich, C.; Gao, H.; Grunenfelder, D.; Hao, H. X.; Jacob, J.; Ho, S.; Hsiao, K.; Kang, Z. B.; Karki, R.; Kato, M.; Larrow, J.; La Bonte, L. R.; Lenoir, F.; Liu, G.; Liu, S.; Majumdar, D.; Meyer, M. J.; Palermo, M.; Perez, L.; Pu, M.; Price, E.; Quinn, C.; Shakya, S.; Shultz, M. D.; Slisz, J.; Venkatesan, K.; Wang, P.; Warmuth, M.; Williams, S.; Yang, G.; Yuan, J.; Zhang, J. H.; Zhu, P.; Ramsey, T.; Keen, N. J.; Sellers, W. R.; Stams, T.; Fortin, P. D. Allosteric inhibition of SHP2 phosphatase inhibits cancers driven by receptor tyrosine kinases. *Nature* **2016**, *535*, 148−152.
(5) Okazaki, T.; Maeda, A.; Nishimura, H.; Kurosaki, T.; Honjo, T. PD-1 immunoreceptor inhibits B cell receptor-mediated signaling by recruiting src homology 2-domain-containing tyrosine phosphatase 2 to phosphotyrosine. *Proc. Natl. Acad. Sci. U. S. A.* **2001**, *98*, 13866−13871.
(6) Zhao, M.; Guo, W.; Wu, Y.; Yang, C.; Zhong, L.; Deng, G.; Zhu, Y.; Liu, W.; Gu, Y.; Lu, Y.; Kong, L.; Meng, X.; Xu, Q.; Sun, Y. SHP2 inhibition triggers anti-tumor immunity and synergizes with PD-1 blockade. *Acta Pharm. Sin. B* **2019**, *9*, 304−315.
(7) Liu, C.; Lu, H.; Wang, H.; Loo, A.; Zhang, X.; Yang, G.; Kowal, C.; Delach, S.; Wang, Y.; Goldoni, S.; Hastings, W. D.; Wong, K.; Gao, H.; Meyer, M. J.; Moody, S. E.; LaMarche, M. J.; Engelman, J. A.; Williams, J. A.; Hammerman, P. S.; Abrams, T. J.; Mohseni, M.; Caponigro, G.; Hao, H. X. Combinations with Allosteric SHP2 Inhibitor TNO155 to Block Receptor Tyrosine Kinase Signaling. *Clin. Cancer Res.* **2021**, *27*, 342−354.
(8) LaRochelle, J. R.; Fodor, M.; Xu, X.; Durzynska, I.; Fan, L.; Stams, T.; Chan, H. M.; LaMarche, M. J.; Chopra, R.; Wang, P.; Fortin, P. D.; Acker, M. G.; Blacklow, S. C. Structural and Functional Consequences of Three Cancer-Associated Mutations of the Oncogenic Phosphatase SHP2. *Biochemistry* **2016**, *55*, 2269−2277.
(9) Tsutsumi, R.; Ran, H.; Neel, B. G. Off-target inhibition by active site-targeting SHP2 inhibitors. *FEBS Open Bio* **2018**, *8*, 1405−1411.
(10) Yuan, X.; Bu, H.; Zhou, J.; Yang, C. Y.; Zhang, H. Recent Advances of SHP2 Inhibitors in Cancer Therapy: Current Development and Clinical Application. *J. Med. Chem.* **2020**, *63*, 11368−11396.
(11) Garcia Fortanet, J.; Chen, C. H.; Chen, Y. N.; Chen, Z.; Deng, Z.; Firestone, B.; Fekkes, P.; Fodor, M.; Fortin, P. D.; Fridrich, C.; Grunenfelder, D.; Ho, S.; Kang, Z. B.; Karki, R.; Kato, M.; Keen, N.; LaBonte, L. R.; Larrow, J.; Lenoir, F.; Liu, G.; Liu, S.; Lombardo, F.; Majumdar, D.; Meyer, M. J.; Palermo, M.; Perez, L.; Pu, M.; Ramsey, T.; Sellers, W. R.; Shultz, M. D.; Stams, T.; Towler, C.; Wang, P.; Williams, S. L.; Zhang, J. H.; LaMarche, M. J. Allosteric Inhibition of SHP2: Identification of a Potent, Selective, and Orally Efficacious Phosphatase Inhibitor. *J. Med. Chem.* **2016**, *59*, 7773−7782.
(12) Nichols, R. J.; Haderk, F.; Stahlhut, C.; Schulze, C. J.; Hemmati, G.; Wildes, D.; Tzitzilonis, C.; Mordec, K.; Marquez, A.; Romero, J.; Hsieh, T.; Zaman, A.; Olivas, V.; McCoach, C.; Blakely, C. M.; Wang, Z.; Kiss, G.; Koltun, E. S.; Gill, A. L.; Singh, M.; Goldsmith, M. A.; Smith, J. A. M.; Bivona, T. G. RAS nucleotide cycling underlies the SHP2 phosphatase dependence of mutant BRAF-, NF1- and RAS-driven cancers. *Nat. Cell Biol.* **2018**, *20*, 1064−1073.
(13) LaMarche, M. J.; Acker, M.; Argintaru, A.; Bauer, D.; Boisclair, J.; Chan, H.; Chen, C. H.; Chen, Y. N.; Chen, Z.; Deng, Z.; Dore, M.; Dunstan, D.; Fan, J.; Fekkes, P.; Firestone, B.; Fodor, M.; Garcia-Fortanet, J.; Fortin, P. D.; Fridrich, C.; Giraldes, J.; Glick, M.; Grunenfelder, D.; Hao, H. X.; Hentemann, M.; Ho, S.; Jouk, A.; Kang, Z. B.; Karki, R.; Kato, M.; Keen, N.; Koenig, R.; LaBonte, L. R.; Larrow, J.; Liu, G.; Liu, S.; Majumdar, D.; Mathieu, S.; Meyer, M. J.; Mohseni, M.; Ntaganda, R.; Palermo, M.; Perez, L.; Pu, M.; Ramsey, T.; Reilly, J.; Sarver, P.; Sellers, W. R.; Sendzik, M.; Shultz, M. D.; Slisz, J.; Slocum, K.; Smith, T.; Spence, S.; Stams, T.; Straub, C.; Tamez, V., Jr.; Toure, B.

B.; Towler, C.; Wang, P.; Wang, H.; Williams, S. L.; Yang, F.; Yu, B.; Zhang, J. H.; Zhu, S. Identification of TNO155, an Allosteric SHP2 Inhibitor for the Treatment of Cancer. *J. Med. Chem.* **2020**, *63*, 13578−13594.

(14) Ma, C.; Gao, P.; Hu, S.; Xu, Z.; Han, H.; Wu, X.; Kang, D. Novel heterocyclic derivatives useful as SHP2 inhibitors. WO 2018172984, 2018.

(15) Ou, S. I.; Koczywas, M.; Ulahannan, S.; Janne, P.; Pacheco, J.; Burris, H.; McCoach, C.; Wang, J. S.; Gordon, M.; Haura, E.; Riess, J. W.; Zhu, V.; Ng, K.; Eckhardt, S. G.; Capasso, A.; Dua, R.; Chen, A.; Wang, Z.; Hayes, J.; Nichols, R.; Bivona, T. The SHP2 Inhibitor RMC-4630 in Patients with KRAS-Mutant Non-Small Cell Lung Cancer: Preliminary Evaluation of a First-in-Man Phase 1 Clinical Trial. Sixth AACR-IASLC International Joint Conference: Lung Cancer Translational Science from the Bench to the Clinic, January 11−14, 2020, San Diego, CA; Poster A12.

(16) Albrecht, B. K.; Giordanetto, F.; Greisman, J. B.; Maragakis, P.; Taylor, A. M.; Walters, P. SHP2 Phosphatase inhibitors and methods of use thereof. WO 2018057884, 2018.

(17) Lu, H.; Liu, C.; Huynh, H.; Le, T. B. U.; LaMarche, M. J.; Mohseni, M.; Engelman, J. A.; Hammerman, P. S.; Caponigro, G.; Hao, H. X. Resistance to allosteric SHP2 inhibition in FGFR-driven cancers through rapid feedback activation of FGFR. *Oncotarget* **2020**, *11*, 265−281.

(18) Aay, N.; Buckl, A.; Gill, A.; Jogalekar, A.; Kiss, G.; Koltun, E. S.; Mellem, K.; Semko, C.; Won, W. *2,5-Disubstituted 3-Methyl Pyrazines and 2,5,6-Trisubstituted 3-Methyl Pyrazines as Allosteric Shp2 Inhibitors*; Revolution Medicines Inc., 2019.

(19) Donovan, K. A.; An, J.; Nowak, R. P.; Yuan, J. C.; Fink, E. C.; Berry, B. C.; Ebert, B. L.; Fischer, E. S. Thalidomide promotes degradation of SALL4, a transcription factor implicated in Duane Radial Ray syndrome. *eLife* **2018**, *7*, e38430.

(20) Kabsch, W. Xds. *Acta Crystallogr., Sect. D: Biol. Crystallogr.* **2010**, *66*, 125−132.

(21) Emsley, P.; Cowtan, K. Coot: model-building tools for molecular graphics. *Acta Crystallogr., Sect. D: Biol. Crystallogr.* **2004**, *60*, 2126−2132.

(22) Afonine, P. V.; Grosse-Kunstleve, R. W.; Echols, N.; Headd, J. J.; Moriarty, N. W.; Mustyakimov, M.; Terwilliger, T. C.; Urzhumtsev, A.; Zwart, P. H.; Adams, P. D. Towards automated crystallographic structure refinement with phenix.refine. *Acta Crystallogr., Sect. D: Biol. Crystallogr.* **2012**, *68*, 352−367.

(23) Moriarty, N. W.; Grosse-Kunstleve, R. W.; Adams, P. D. electronic Ligand Builder and Optimization Workbench (eLBOW): a tool for ligand coordinate and restraint generation. *Acta Crystallogr., Sect. D: Biol. Crystallogr.* **2009**, *65*, 1074−1080.

(24) Chen, V. B.; Arendall, W. B., 3rd; Headd, J. J.; Keedy, D. A.; Immormino, R. M.; Kapral, G. J.; Murray, L. W.; Richardson, J. S.; Richardson, D. C. MolProbity: all-atom structure validation for macromolecular crystallography. *Acta Crystallogr., Sect. D: Biol. Crystallogr.* **2010**, *66*, 12−21.

(25) Morin, A.; Eisenbraun, B.; Key, J.; Sanschagrin, P. C.; Timony, M. A.; Ottaviano, M.; Sliz, P. Collaboration gets the most out of software. *eLife* **2013**, *2*, No. e01456.

(26) Lin, K. M.; Lin, S. J.; Lin, J. H.; Lin, P. Y.; Teng, P. L.; Wu, H. E.; Yeh, T. H.; Wang, Y. P.; Chen, M. R.; Tsai, C. H. Dysregulation of Dual-Specificity Phosphatases by Epstein-Barr Virus LMP1 and Its Impact on Lymphoblastoid Cell Line Survival. *J. Virol.* **2020**, *94*, e01837-19.

(27) Winter, G. E.; Buckley, D. L.; Paulk, J.; Roberts, J. M.; Souza, A.; Dhe-Paganon, S.; Bradner, J. E. DRUG DEVELOPMENT. Phthalimide conjugation as a strategy for in vivo target protein degradation. *Science* **2015**, *348*, 1376−1381.

(28) Vannam, R.; Sayilgan, J.; Ojeda, S.; Karakyriakou, B.; Hu, E.; Kreuzer, J.; Morris, R.; Herrera Lopez, X. I.; Rai, S.; Haas, W.; Lawrence, M.; Ott, C. J. Targeted degradation of the enhancer lysine acetyltransferases CBP and p300. *Cell Chem. Biol.* **2021**, *28*, 503.

(29) Wang, L.; Shao, X.; Zhong, T.; Wu, Y.; Xu, A.; Sun, X.; Gao, H.; Liu, Y.; Lan, T.; Tong, Y.; Tao, X.; Du, W.; Wang, W.; Chen, Y.; Li, T.; Meng, X.; Deng, H.; Yang, B.; He, Q.; Ying, M.; Rao, Y. Discovery of a first-in-class CDK2 selective degrader for AML differentiation therapy. *Nat. Chem. Biol.* **2021**, *17*, 567.

(30) Zhang, F.; Wu, Z.; Chen, P.; Zhang, J.; Wang, T.; Zhou, J.; Zhang, H. Discovery of a new class of PROTAC BRD4 degraders based on a dihydroquinazolinone derivative and lenalidomide/pomalidomide. *Bioorg. Med. Chem.* **2020**, *28*, 115228.

(31) LaRochelle, J. R.; Fodor, M.; Vemulapalli, V.; Mohseni, M.; Wang, P.; Stams, T.; LaMarche, M. J.; Chopra, R.; Acker, M. G.; Blacklow, S. C. Structural reorganization of SHP2 by oncogenic mutations and implications for oncoprotein resistance to allosteric inhibition. *Nat. Commun.* **2018**, *9*, 4508.

(32) Zhang, D.; Baek, S. H.; Ho, A.; Kim, K. Degradation of target protein in living cells by small-molecule proteolysis inducer. *Bioorg. Med. Chem. Lett.* **2004**, *14*, 645−648.

(33) Zorba, A.; Nguyen, C.; Xu, Y.; Starr, J.; Borzilleri, K.; Smith, J.; Zhu, H.; Farley, K. A.; Ding, W.; Schiemer, J.; Feng, X.; Chang, J. S.; Uccello, D. P.; Young, J. A.; Garcia-Irrizary, C. N.; Czabaniuk, L.; Schuff, B.; Oliver, R.; Montgomery, J.; Hayward, M. M.; Coe, J.; Chen, J.; Niosi, M.; Luthra, S.; Shah, J. C.; El-Kattan, A.; Qiu, X.; West, G. M.; Noe, M. C.; Shanmugasundaram, V.; Gilbert, A. M.; Brown, M. F.; Calabrese, M. F. Delineating the role of cooperativity in the design of potent PROTACs for BTK. *Proc. Natl. Acad. Sci. U. S. A.* **2018**, *115*, E7285−E7292.

(34) Wang, B.; Wu, S.; Liu, J.; Yang, K.; Xie, H.; Tang, W. Development of selective small molecule MDM2 degraders based on nutlin. *Eur. J. Med. Chem.* **2019**, *176*, 476−491.

(35) Li, Y.; Yang, J.; Aguilar, A.; McEachern, D.; Przybranowski, S.; Liu, L.; Yang, C. Y.; Wang, M.; Han, X.; Wang, S. Discovery of MD-224 as a First-in-Class, Highly Potent, and Efficacious Proteolysis Targeting Chimera Murine Double Minute 2 Degrader Capable of Achieving Complete and Durable Tumor Regression. *J. Med. Chem.* **2019**, *62*, 448−466.

(36) Wang, M.; Lu, J.; Wang, M.; Yang, C. Y.; Wang, S. Discovery of SHP2-D26 as a First, Potent, and Effective PROTAC Degrader of SHP2 Protein. *J. Med. Chem.* **2020**, *63*, 7510−7528.

(37) Yang, X.; Wang, Z.; Pei, Y.; Song, N.; Xu, L.; Feng, B.; Wang, H.; Luo, X.; Hu, X.; Qiu, X.; Feng, H.; Yang, Y.; Zhou, Y.; Li, J.; Zhou, B. Discovery of thalidomide-based PROTAC small molecules as the highly efficient SHP2 degraders. *Eur. J. Med. Chem.* **2021**, *218*, 113341.

https://doi.org/10.1021/acs.biochem.1c00377
Biochemistry 2021, 60, 2593−2609